MATHEMATICAL MODELING OF FBCs CO-FIRED WITH LIGNITE AND BIOMASS

A THESIS SUBMITTED TO
THE GRADUATE SCHOOL OF NATURAL AND APPLIED SCIENCES
OF
MIDDLE EAST TECHNICAL UNIVERSITY

BY

EKREM MEHMET MORALI

IN PARTIAL FULFILLMENT OF THE REQUIREMENTS
FOR
THE DEGREE OF MASTER OF SCIENCE
IN
CHEMICAL ENGINEERING

JULY 2007

Approval of the thesis:

MATHEMATICAL MODELING OF FBCs CO-FIRED WITH LIGNITE AND BIOMASS

submitted by **EKREM MEHMET MORALI** in partial fulfillment of the requirements for the degree of **Master of Science in Chemical Engineering Department, Middle East Technical University** by,

Prof. Dr. Canan Özgen _____
Dean, Graduate School of **Natural and Applied Sciences**

Prof. Dr. Nurcan Baç _____
Head of Department, **Chemical Engineering**

Prof. Dr. Nevin Selçuk _____
Supervisor, **Chemical Engineering Dept., METU**

Asst. Prof. Dr. Görkem Külah _____
Co-Supervisor, **Chemical Engineering Dept., METU**

Examining Committee Members:

Prof. Dr. Nurcan Baç _____
Chemical Engineering Dept., METU

Prof. Dr. Nevin Selçuk _____
Chemical Engineering Dept., METU

Asst. Prof. Dr. Görkem Külah _____
Chemical Engineering Dept., METU

Prof. Dr. Yavuz Samim Ünlüsoy _____
Mechanical Engineering Dept., METU

Ümit Kırmızıgül (M.Sc.) _____
Mimag-Samko

Date: 27.07.2007

I hereby declare that all information in this document has been obtained and presented in accordance with academic rules and ethical conduct. I also declare that, as required by these rules and conduct, I have fully cited and referenced all material and results that are not original to this work.

Name, Last name : Ekrem Mehmet Moralı

Signature :

ABSTRACT

MATHEMATICAL MODELING OF FBCs CO-FIRED WITH LIGNITE AND BIOMASS

Moralı, Ekrem Mehmet

M.Sc., Department of Chemical Engineering

Supervisor: Prof. Dr. Nevin Selçuk

Co-Supervisor: Asst. Prof. Dr. Görkem Külah

July 2007, 79 pages

Increasing environmental legislations on pollutant emissions originated from fossil fuel combustion and intention of increasing the life of existing fossil fuels give rise to the use of renewable sources. Biomass at this juncture, with its renewable nature and lower pollutant emission levels becomes an attractive energy resource. However, only seasonal availability of biomass and operation problems caused by high alkaline content of biomass ash restrict its combustion alone. These problems can be overcome by co-combustion of biomass with lignite. With its high fuel flexibility and high combustion efficiency, fluidized bed combustion is the most promising technology for co-firing. To improve and optimize the operation of co-firing systems a detailed understanding of co-combustion of coal and biomass is necessary, which can be achieved both with experiments and modeling studies. For this purpose, a comprehensive system model of fluidized bed combustor, previously developed and tested for prediction of combustion behaviour of fluidized bed combustors fired

with lignite was extended to co-firing lignite with biomass by incorporating volatile release, char combustion and population balance for biomass.

The model predictions were validated against experimental measurements taken on METU 0.3 MWt AFBC fired with lignite only, lignite with limestone addition and about 50/50 lignite/olive residue mixture with limestone addition. Predicted and measured temperatures and concentrations of gaseous species along the combustor were found to be in good agreement. Introduction of biomass to lignite was found to decrease SO_2 emissions but did not affect NO emissions significantly.

Keywords: Co-Combustion, Lignite, Biomass, Mathematical modeling

ÖZ

AKIŞKAN YATAKLI YAKICILARIN MATEMATİKSEL MODELLENMESİ LİNYİT VE BİYOKÜTLENİN BERABER YAKILMASI

Moralı, Ekrem Mehmet

Yüksek Lisans, Kimya Mühendisliği Bölümü

Tez Yöneticisi: Prof. Dr. Nevin Selçuk

Ortak Tez Yöneticisi: Yrd. Doç. Dr. Görkem Külah

Temmuz 2007, 79 sayfa

Fosil yakıtların yakılması kaynaklı kirletici gaz emisyonlarının azaltılması yönünde getirilen yasal düzenlemeler yenilenebilir enerji kaynaklarının kullanımını teşvik etmektedir. Bu bağlamda biyokütle yenilenebilir karakteri ve yakımı sonunda düşük kirletici gaz salınımıyla öne çıkmaktadır. Ancak, biyokütlenin sezona bağlı arzı ve yakımı esnasında karşılaşılan işletme sorunları bu yakıtın tek başına kullanımını engellemektedir. Bu sebeplerden dolayı biyokütle ve linyitin beraber yakılması gerekliliği ortaya çıkmaktadır. Beraber yakma süreçleri için yüksek yakıt esnekliği ve yanma verimliliği sebebiyle akışkan yatak teknolojisi öne çıkmaktadır. Beraber yakma sistemlerinin optimize edilmesi ve iyileştirilmesi için beraber yakma sürecinin iyi incelenmesi gerekmektedir. Bu da deneysel ve modelleme çalışmaları ile yapılabilir. Bu amaçla, daha önce geliştirilmiş ve deneysel verilerle sınanmış sistem modeli biyokütle uçucu salınımı, kok yanması ve tane boyutu değişim modellerini kapsayacak şekilde genişletilmiştir.

Model öngörüleri, ODTÜ 0.3 MWt AKAYY test ünitesinde sadece linyit, kireçtaşı katkılı linyit ve ağırlık bazında 50/50 linyit/biyokütle karışımının kireçtaşı katkılı yakılması sırasında elde edilen deney sonuçlarıyla karşılaştırılmıştır. Model sonuçlarının deneyden elde edilen gaz sıcaklıkları ve bileşimleriyle ile iyi uyum içinde olduğu gözlemlenmiştir. Yakıta biyokütle katılmasının SO_2 emisyonlarını düşürdüğü ancak NO emisyonlarını önemli derecede etkilemediği tespit edilmiştir.

Anahtar Kelimeler: Beraber yakma, Linyit, Biyokütle, Matematiksel modelleme

to my family . . .

ACKNOWLEDGEMENTS

I wish to express my deepest gratitude to my supervisor, Prof. Dr. Nevin Selçuk for for her guidance and constant encouragement throughout this study.

I also would like to show my appreciation to my co-supervisor Asst. Prof. Dr. Görkem Külah for her support.

I also thank to AFBC research team members for their friendship and support during my study; Dr. Ahmet Bilge Uygur, Dr. Işıl Ayrancı, Zeynep Serinyel, Ertan Karaismail, Aykan Batu, Nihan Çayan, Dr. Yusuf Göğebakan, Dr. Tanıl Tarhan, Mehmet Onur Afacan, Düriye Ece Alagöz, Güzide Aydın and Zuhal Göğebakan.

Besides members of AFBC research team my thanks go to my friends Onur Kaçar, Engin Özkol, Gül Çorbacıoğlu and Erinç Bahçegül.

Finally, I would like to thank my family for their tolerance and patience, and encouragement.

TABLE OF CONTENTS

LIST OF TABLES

TABLES

LIST OF FIGURES

FIGURES

LIST OF SYMBOLS

a	Decay constant, cm^{-1}
A	Cross-sectional area, cm^2
c_p	Specific heat capacity, $cal\ g^{-1}\ K^{-1}$
C	Concentration, $mol\ cm^{-3}$
d	Diameter, cm
D	Diffusivity of oxygen in nitrogen, $cm^2\ s^{-1}$
E	Activation energy, $cal\ mol^{-1}$
$E(r)$	Elutriation rate constant, s^{-1}
$f(E)$	Activation energy distribution function for devolatilization, $mol\ cal^{-1}$
F	Char flow rate, $g\ s^{-1}$
F_z	Upward flow rate of entrained particles at any height z in freeboard, $g\ s^{-1}$
g	Gravitational acceleration, $cm\ s^{-2}$
h	Individual heat transfer coefficient, $cal\ cm^{-2}\ s^{-1}\ K^{-1}$
H	Height, cm
ΔH^0	Heat of reaction at standard state, $cal\ mol^{-1}$
k	Overall sulfation rate constant, cm/s; thermal conductivity, $cal\ cm^{-1}\ s^{-1}\ K^{-1}$
$k(E)$	First-order reaction rate constant for devolatilization, s^{-1}
k_C	Reaction rate constant for char combustion, $cm\ s^{-1}$
k_{CO}	Reaction rate constant for CO oxidation, $(cm^3\ mol^{-1})^{0.8}\ s^{-1}$
k_f	Film mass transfer coefficient, $cm\ s^{-1}$
k_s	First order surface reaction rate constant for char combustion, $cm\ s^{-1}$
K	Coal nitrogen partitioning factor
K_{be}	Interphase mass transfer coefficient, s^{-1}
$K^*_{i\infty}$	Dispersed non-cluster flux of entrained particles in size i, $g\ cm^{-2}\ s^{-1}$
K^*_{ih}	Cluster flux of entrained particles in size i, $g\ cm^{-2}\ s^{-1}$

K_i^*	Total flux of entrained particles in size *i*, *g* cm^{-2} s^{-1}
L	Length, *cm*
m	Mass flow rate, *g* s^{-1}
M	Molecular or atomic weight, *g* mol^{-1}; hold-up in the bed, *g*
n	Index of the dimension; molar flow rate, *mol* s^{-1}
n_C	Carbon consumption rate, *mol* cm^{-3} s^{-1}
n_N	Char nitrogen oxidation rate, *mol* cm^{-3} s^{-1}
N_r	Number of cycles of recycled sorbent and ash particles
$P(r)$	Size distribution function, cm^{-1}
$P_z(r)$	Size distribution of entrained particles at any height *z* in freeboard, cm^{-1}
Q	Volumetric flow rate, cm^3 s^{-1}; energy generation/loss rate, *cal* s^{-1}
r	Spatial independent variable, *cm*
r_C	Carbon consumption rate on the surface of char particle, *mol* cm^{-2} s^{-1}
r_N	Char nitrogen oxidation rate on the surface of char particle, *mol* cm^{-2} s^{-1}
r_{CO}	Rate of CO combustion, *mol* cm^{-3} s^{-1}
r_{SO_2}	Rate of sulfation reaction, *mol* s^{-1}
r_{NO}	Rate of heterogeneous reaction over single particle of size r, *mol* $g^{-1}s^{-1}$
$r_{N,het}$	Rate of heterogeneous reaction, *mol* s^{-1}
$r_{N,hom}$	Rate of homogeneous reaction, R10: *mol* cm^{-3} s^{-1}; R11: *mol* s^{-1}
R	Ideal gas constant, *cal* mol^{-1} K^{-1}; radius, *cm*
$\boldsymbol{R}$	Energy generation/loss rate in freeboard, *cal* cm^{-3} s^{-1}
$\Re$	Species generation/depletion rate, *mol* cm^{-3} s^{-1}
$\Re(r)$	Shrinkage rate of char particles, *cm* s^{-1}
Re_p	Particle Reynolds number, -
R_w	Thermal resistance across the freeboard wall, *cal* cm^{-2} s^{-1} K^{-1}
S	External sorbent surface area, cm^2
t	Time, *s*
T	Temperature, *K*
u_0	Superficial velocity in the bed, *cm* s^{-1}
u_b	Superficial bubble phase velocity, *cm* s^{-1}
u_e	Superficial velocity in emulsion phase, *cm* s^{-1}

u_{mf} Superficial minimum fluidization velocity, $cm\ s^{-1}$

u_t Terminal velocity of the particles, $cm\ s^{-1}$

u_{tf} Superficial throughflow velocity in bubbles, $m\ s^{-1}$

U Overall heat transfer coefficient, $cal\ cm^{-2}\ s^{-1}\ K^{-1}$

U_f Unit filter function

V Volume, cm^3

W_N Mass of char nitrogen, g

X_{NH_3} Molar ratio of NH_3 in the volatile nitrogen

x Mass fraction (dry basis); spatial independent variable, cm

x_{vl} Fraction of volatiles released in the bed

y Mole fraction

z Spatial independent variable, cm

Greek Letters

α Thermal diffusivity, $cm^2\ s^{-1}$

δ Bubble phase volume fraction

ε Voidage; emissivity; convergence criterion

ε_f Voidage at fluidization conditions

ε_{mf} Voidage at minimum fluidization conditions

ε_s Solids volume fraction

η Contact efficiency

λ^0 Latent heat of vaporization at standard state, $cal\ g^{-1}$

μ Viscosity, $g\ cm^{-1}\ s^{-1}$

ρ Density, $g\ cm^3$

σ Standard deviation of activation energy distribution, $J\ mol^{-1}$; Stephan-Boltzman constant, $cal\ cm^{-2}\ s^{-1}\ K^{-4}$; Fractional sorbent surface area

v Volatiles released, %

v_∞ Ultimate yield of volatiles released, %

ϕ Sphericity, -

Subscripts

32	Surface/volume mean
a	Air; ash; attrition
avg	Average
b	Bubble
bd	Bed drain
bed	Bed
bio	Biomass orginated
bw	Bed wall
c	Combustion
C	Carbon
co	Carryover
coal	Coal orginated
cw	Cooling water
d	Char
e	Emulsion
elut	Elutriation
f	Freeboard; fine; feed coal
fc	Fixed carbon
fw	Freeboard wall
G	Gas
H	Hydrogen
het	heterogeneous
hom	homogeneous
I	Inert; inner
J	Species index
lst	Limestone
max	Maximum
maxe	Maximum elutriated
min	Minimum
o	Feed; outer; at the bed surface; initial
p	Particle

r	Radiation; reference
recy	Recycle
rxn	Reaction
S	Sulfur
s	Surface; solid
T	Tube
vm	Volatile matter
w	Wall; water

Abbreviations

d.a.f.	dry ash free
ABFBC	Atmospheric Bubbling Fluidized Bed Combustor
AFBC	Atmospheric Fluidized Bed Combustor
FBC	Fluidized Bed Combustion
FC	Fixed Carbon
GC	Gas Chromotography
OHTC	Overall Heat Transfer Coefficient
TGA	Thermogravimetric Analyzer
VM	Volatile Matter

CHAPTER 1

INTRODUCTION

Coal is the most abundant and almost uniformly distributed fuel in the world. Current reserves of coal are approximately four times the reserves of oil and gas. It will therefore be used in the future for energy production, in an attempt to cope with the increasing energy demand. Turkey has widely spread indigenous sources of lignite reserves. However, it is characterized with its high volatile matter, sulfur and ash content.

In order to comply with the sustainable energy policy, efficient and clean combustion of coal has become one of the most pressing goals of combustion engineering, and hence clean combustion of low quality lignite should be ensured. To achieve this purpose, fluidized bed combustion comes into picture as a clean coal combustion technology with lower operating temperature, in-situ desulphurization, acceptable levels of gaseous pollutant emissions, high availability and high heat transfer coefficients. Moreover, fluidized bed combustors possess the advantage of handling low quality, high sulphur content coals, which makes them suitable for Turkish lignite.

On the other hand increasing legislations on pollutant emissions for combustion systems promoted the interest of utilizing alternative sources for energy production. Biomass, at this juncture with its renewable nature and lower pollutant emission levels becomes an attractive energy source. The term biomass describes carbonaceous materials derived from renewable plants, which result in solid fuels with high volatile matter content and high calorific value. Some examples include olive residue, hazelnut shells, rice shafts and straw.

In Turkey, especially olive residue, which is the remaining part of olive after milling and extraction of the olive oil, is produced in large quantities as Turkey is a major olive producer. Olive residue can be fired for energy production. However, one of the main problems regarding the utilization of olive residue as a source of energy alone, like other biomass kinds, is its seasonal supply, since it is a natural waste and its supply varies depending on the season. In addition to limitation regarding seasonal supply, burning biomass alone causes also operating problems:

- Corrosion: The ash of biomass contains high content of alkali compounds. If the biomass contains high amounts of chlorine, this may react with bed material to give HCl, which is a highly corrosive substance.
- Bed agglomeration: Low melting point of biomass ash may cause agglomeration in the bed.
- Slagging and fouling: Bed ash deposit on heat transfer surfaces causes low heat transfer coefficients, resulting in a decrease of the thermal efficiency of the system.

Given the possibility of encountering these operating problems with biomass, burning biomass alone is not feasible. This leads us to the co-firing of biomass with lignite. FBC is a good candidate for this purpose due to its high fuel flexibility. In the literature, there are a number of experimental studies, on co-combustion of biomass and coal in fluidized bed combustors (FBCs), [1–5], however there exist a limited number of studies of mathematical modeling of co-combustion of coal with biomass. Okasha [6] has presented a steady-state model for bubbling fluidized bed combustion of straw-bitumen pellets, which is an alternative fuel proposed by the same author. In this model, hydrodynamics, volatile release, char particle combustion and entrainment are taken into considerations. Main shortcomings of the model are absence of char population balance and pollutant species balances. Findings are limited to over-bed feeding of pellets of 15 *mm* diameter and 15 *mm* length compressed under pressure of 150 *bar* are made of a 1:1 blend of rice straw

and bitumen and hence the feasibility of adaption to industrial scale is questionable. Model predictions were found to be in good agreement with measurements from a 0.3 m ID, 3.3 m height atmospheric bubbling fluidized bed combustor burning straw-bitumen pellets in silica sand.

Another modeling study was carried out by Adanez *et al.* [7] for a 0.3 MWt circulating fluidized bed combustor, co-firing coal with a forest residue, i.e. pine bark. In this model, hydrodynamics, devolatilization, char population balances, char and volatile combustion are taken into consideration. However, sulfur retention and NO formation is not taken into consideration.

Despite having limited number of modeling studies, a comprehensive model for co-firing of biomass and coal as separate solid streams in a bubbling FBC is not available to date.

Therefore, absence of a comprehensive model for co-firing of biomass and lignite on one hand, and recent in utilization of alternative sources like biomass for energy production on the other, necessitated the development of a comprehensive model for FBCs co-fired with lignite and biomass. In this study, a previously developed comprehensive system model, originally proposed by Selçuk and Sivrioğlu [8] and later improved, extended and validated against experimental data by Selçuk and her colleagues [9], is chosen as a basis for modeling of biomass-lignite co-combustion in bubbling fluidized bed combustor. The predictive performance of the model is tested by comparing the its predictions with on-line concentration measurements of O_2, CO_2, CO and NO along the METU 0.3 MWt Atmospheric Bubbling Fluidized Bed Combustor, where typical Turkish lignite is co-fired with olive residue.

CHAPTER 2

SYSTEM MODEL FOR ABFBC CO-FIRING LIGNITE WITH BIOMASS

2.1 General

In this thesis study, a comprehensive system model on fluidized bed combustion, originally proposed by Selçuk and Sivrioğlu [8] and later extended and validated against experimental data by Selçuk and her colleagues [9, 10] was chosen as basis for modeling of co-combustion. The model in its original form accounts for bed and freeboard hydrodynamics, volatiles release and combustion, char particles combustion, particle size distribution, sorbent and ash particles, attrition, sulfur retention and NO formation and reduction. Details of the original model can be found elsewhere [11]. This model is extended to co-firing coal with biomass incorporating particle size distribution, volatile release, char combustion, mass and energy balances. The main assumptions for bed and freeboard sections of the system model are illustrated in Figure 2.1 and Figure 2.2.

The behaviour of the fluidized bed combustor under consideration is described by a model based on conservation equations for energy and chemical species in conservative form for both bed and freeboard sections. Seven chemical species, O_2, CO, CO_2, H_2O, SO_2, NH_3 and NO are considered in the system model. Chemical reactions considered in the model are listed in Table 2.1 and correlations used in estimating important parameters in the model are listed in Table 2.2. The extended model is described in the following sections.

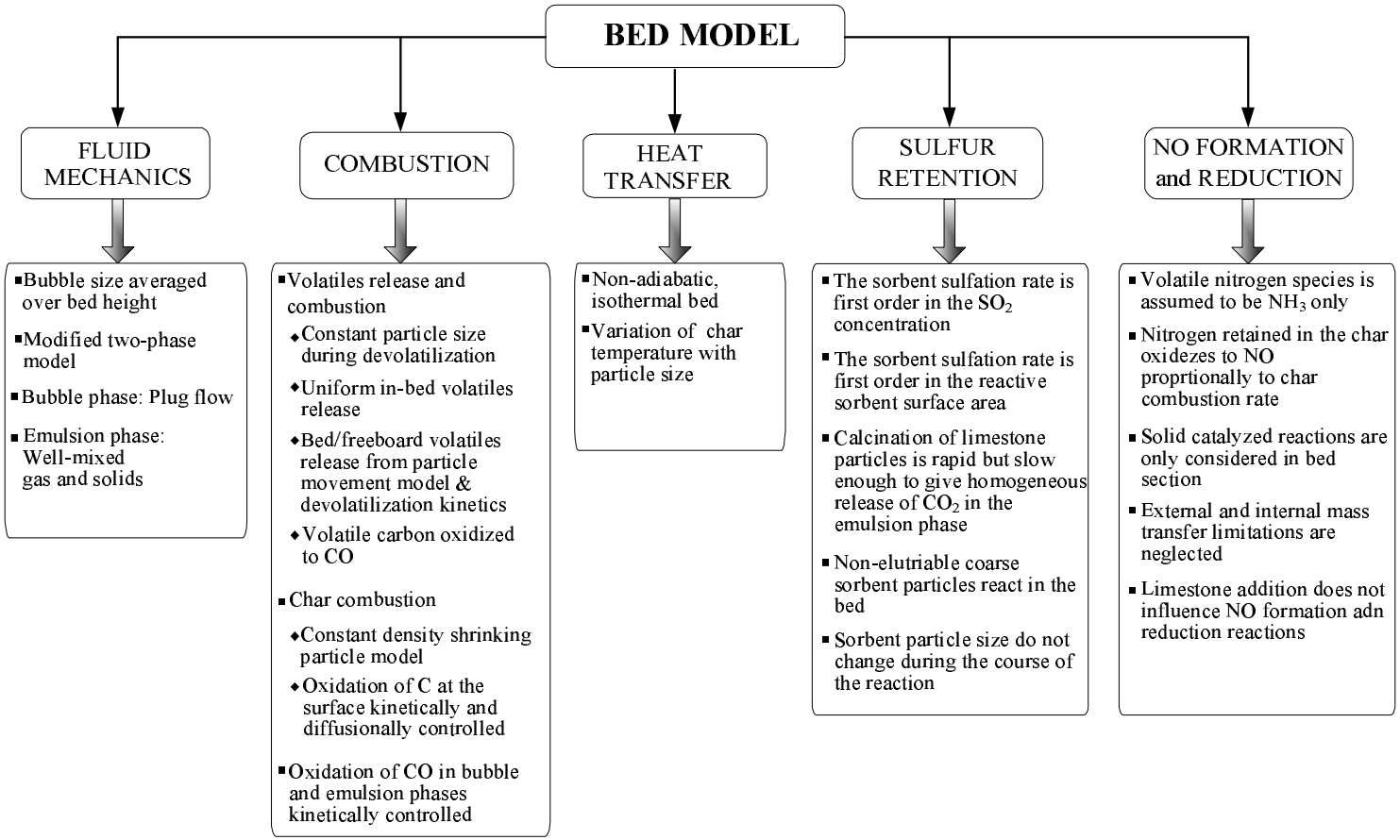

Figure 2.1: Overview of steady state bed model assumptions

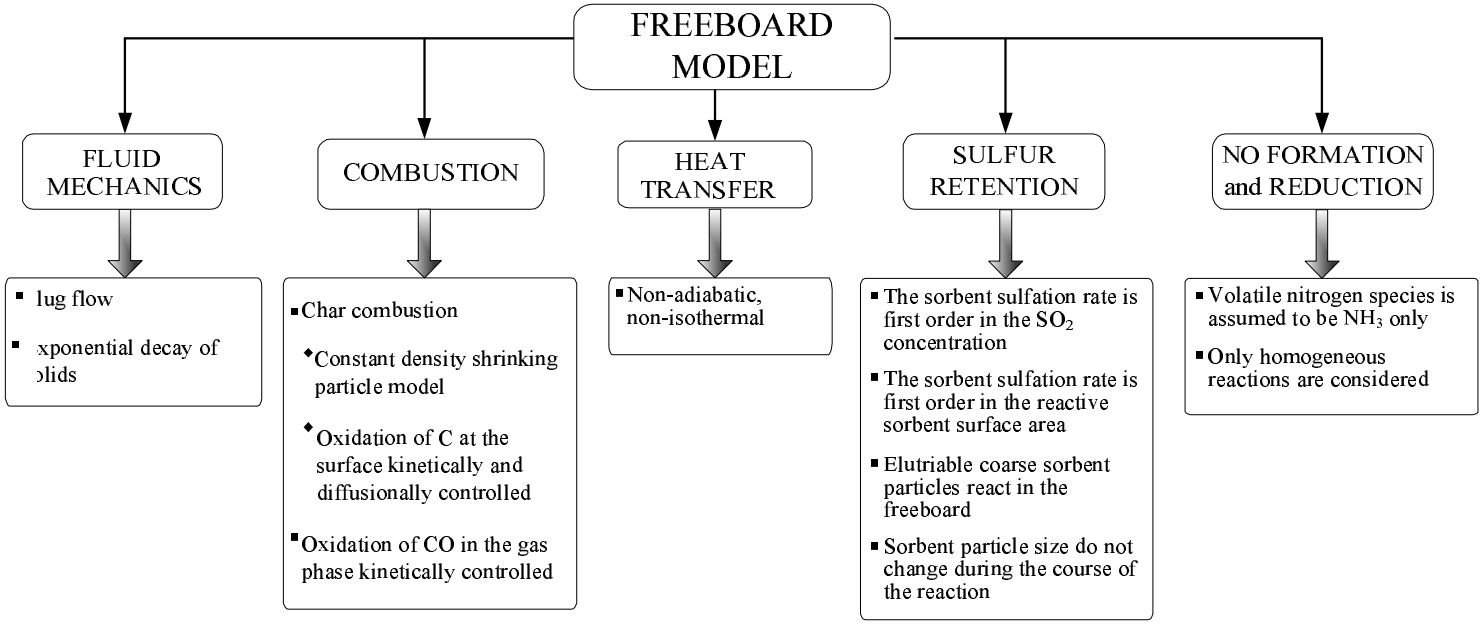

Figure 2.2: Overview of steady state freeboard model assumptions

Table 2.1: Reactions and rate expressions.

	Reaction	Place	Rate expression	unit	Ref.
R1	$C_{scoal} + 1/2O_2 \rightarrow CO$	char surface	$5.95 \times 10^4 T_p exp(-17967/T_p) C_{O2,s}$	$molcm^{-3}s^{-1}$	[12]
	$C_{sbio} + 1/2O_2 \rightarrow CO$	char surface	$250 T_p exp(-16013/T_p) C_{O2,s}$	$molcm^{-3}s^{-1}$	[13]
R2	$C + 1/2O_2 \rightarrow CO$	gas phase	Instantaneous	-	-
R3	$CO + 1/2O_2 \rightarrow CO2$	gas phase	$3.0 \times 10^{10} T \exp(-8052/T_g) C_{0_2}^{0.3} C_{CO} C_{H_2O}^{0.5}$	$molcm^{-3}s^{-1}$	[14]
R4	$H_2 + 1/2O_2 \rightarrow H_2O$	gas phase	Instantaneous	-	-
R5	$S + O_2 \rightarrow SO_2$	gas phase	Instantaneous	-	-
R6	$CaCO_3 \rightarrow CaO + CO_2$	sorbent surface	Instantaneous	-	-
R7	$CaO + SO_2 + 1/2O_2 \rightarrow CaSO_4$	sorbent surface	$14.9 C_{SO_2} S_o \sigma_{avg}$	$mols^{-1}$	[15]
R8	$N_{vol} + 3/2H_2 \rightarrow NH_3$	gas phase	Instantaneous	-	-
R9	$N_s + 1/2O_2 \rightarrow NO$	char surface	proportional to char combustion rate	$molcm^{-3}s^{-1}$	-
R10	$NH_3 + 5/4O_2 \rightarrow NO + 3/2H_2O$	gas phase	$2.21 \times 10^{14} \exp(-38160/T_g) C_{NH_3}$	$molcm^{-3}s^{-1}$	[16]
R11	$NO + 2/3NH_3 \rightarrow 5/6N_2 + H_2O$	gas phase	$2.45 \times 10^{26} \exp(-27680/T_g) C_{NO} C_{NH_3}$	$mols^{-1}$	[16]
R12	$NO + Char \rightarrow 1/2N_2 + CO$	char surface	$3.45 \times 10^6 \exp(-22200/T_d) C_{NO}^{0.52}$	$molg^{-1}s^{-1}$	[17]
R13	$NO + CO \rightarrow CO_2 + 1/2N_2$	char surface	$3.81 \times 10^9 \exp(-22800/T_d) C_{NO}^{0.39} C_{CO}^{0.53}$	$molg^{-1}s^{-1}$	[17]
R14	$NH_3 + 5/4O_2 \rightarrow NO + 3/2H_2O$	char surface	$3.4 \times 10^{10} C_{NH_3} C_{O_2}$	$molg^{-1}s^{-1}$	[17]
R15	$NH_3 + 5/4O_2 \rightarrow NO + 3/2H_2O$	ash surface	$0.4 C_{NH_3}^{0.57} C_{O_2}^{0.11}$	$molg^{-1}s^{-1}$	[17]
R16	$NH_3 + 3/4O_2 \rightarrow 1/2N_2 + 3/2H_2O$	char surface	$8.4 \times 10^{10} C_{NH_3} C_{O_2}$	$molg^{-1}s^{-1}$	[17]
R17	$NH_3 + 3/4O_2 \rightarrow 1/2N_2 + 3/2H_2O$	ash surface	$3.92 \times 10^9 C_{NH_3}^{1.8} C_{O_2}^{0.07}$	$molg^{-1}s^{-1}$	[17]

Table 2.2: Correlations used in the system model.

	Reference
Mass transfer to particles in the emulsion phase, k_f	[18]
Heat transfer to particles in the emulsion phase, h_p	[19]
Specific elutration rate constant, $E(r)$	[20]
Terminal velocity of particles, u_t	[21]
Emulsion phase velocity, u_e	[22]
Minimum fluidization velocity, u_{mf}	[23]
Bubble size, d_b	[24]
Bubble to emulsion mass transfer, K_{be}	[25]
Bubble phase volume fraction, δ	[22]
Convective heat transfer coefficient to bed walls, h_{bw}	[21]
Convective heat transfer coefficient of cooling tubes, h_{cw}	[26]
Convective heat transfer coefficient of cooling water, h_i	[27]
Exponential decay constant, a	[20]
Gas side heat transfer coefficient in freeboard, h_g	[19]

2.2 Bed Model

Bed model can be described in terms of hydrodynamics, volatiles release and combustion, char particles combustion, particle size distribution of char, sorbent and ash particles, attrition, sulfur retention and NO formation and reduction.

2.2.1 Bed Hydrodynamics

Bed hydrodynamics is based on modified two-phase theory suggested by Grace and Clift [28],

$$u_o = \frac{Q_b}{A_{bed}} + u_{tf} + u_e(1-\delta) \tag{2.1}$$

where the throughflow velocity, u_{tf} can be expressed in terms of emulsion phase velocity, u_e, using n-type two phase theory of Grace and Harrison [29]

$$u_{tf} = (n+1)u_e\delta \tag{2.2}$$

For three dimensional beds gas/solid in the emulsion phase and gas in the bubble phase are assumed to be well-stirred and in plug flow, respectively. An integrated average mean bubble size found from bubble size expression proposed by Mori and Wen [24], in the sections unoccupied by the tube bank and from constant and uniform bubble size determined by the clearance between the tubes is utilized. Bubbles are assumed to be free of solids. The gas interchange coefficient between bubble and emulsion phases, K_{be}, is defined as:

$$K_{be} = \frac{\left(\begin{array}{c}\text{volume of gas going from bubbles}\\ \text{to emulsion or from emulsion to bubbles}\end{array}\right)}{(\text{volume of bubbles in the bed})\,(\text{time})} \tag{2.3}$$

To evaluate K_{be}, the following relation was used:

$$K_{be} = 4.5\frac{u_e}{d_b} \tag{2.4}$$

2.2.2 Volatiles Release and Combustion

In the system model volatiles are assumed to be released uniformly in the emulsion phase for both fuels. The need for determination of the amount of volatile matter released in the bed section requires use of volatile release model. There exist two volatile release models in the literature, one proposed by Stubington *et al.* [30], the other one by Fiorentino *et al.* [31].

Stubington's model predicts the location and the quantity of fuel volatiles released in the combustor by combining the results of a particle movement model and time resolved devolatilization profile of coal particles. In this model, it is assumed that particle movement is caused solely by bubbles and that a fuel particle remains

stationary in the bed until a bubble displaces it axially and radially to another stationary point higher up in the bed up to the bed surface.

Another approach was used by Fiorentino *et al.* . In this model, it is assumed that volatiles released by fuel particles form bubbles lifting the particles for their journey in the bed. In other words, volatiles are assumed to be released to the bubbles.

In this thesis study, volatile release model of Stubington *et al.* is deployed due to the fact that it has already been validated successfully by comparing its predictions with experimental data taken on the METU 0.3 MWt ABFBC test rig fired with lignite.

In parallel independent reaction model of Anthony and Howard [32], the volatile release for a particle at radius, r, is given by,

$$\frac{\nu}{\nu_\infty} = 1 - \int_0^\infty \exp\left(-\int_0^t k(E)\,dt\right) f(E)\,dE \tag{2.5}$$

where

$$f(E) = \left[(2\pi)^{1/2}\sigma\right]^{-1} \exp\left[-(E-E_o)^2/2\sigma^2\right] \tag{2.6}$$

$$\int_0^\infty f(E)\,dE = 1 \tag{2.7}$$

$$k(E) = k_o \exp(-E/RT) \tag{2.8}$$

In the presence of radial temperature profile and with assumption of evenly distributed volatile matter in the particle, total amount of volatile matter released as a function of time can be expressed by integrating Eq. (2.5) over particle radius, r:

$$\frac{v_{avg}}{v_\infty} = \frac{3}{R^3}\int_0^R \left[1 - \int_0^\infty \exp\left(-\int_0^t k(E)dt\right) f(E)\,dE\right] r^2 dr \tag{2.9}$$

In order to solve Equation (2.9) the temperature of the particles has to be specified. Assuming devolatilization is thermally neutral, lumped capacitance method is used to determine the temperature of the particle:

$$\frac{\partial T}{\partial t} = \frac{\alpha}{r^2}\frac{\partial}{\partial r}\left(r^2\frac{\partial T}{\partial r}\right) \tag{2.10}$$

where α is thermal diffusivity. The boundary conditions for Equation (2.10) are,

$$\begin{aligned} @r = R \qquad & -k\frac{\partial T}{\partial r} = h_p\left(T_g - T\right) + \sigma\varepsilon\left(T_g^4 - T^4\right) \\ @r = 0 \qquad & \frac{\partial T}{\partial r} = 0 \end{aligned} \tag{2.11}$$

Equation (2.9) contains four parameters to be estimated from experimental data: v_∞, k_0, E_0 and σ, which represents ultimate yield of volatiles, pre-exponential factor, mean activation energy and its standard deviation, respectively.

Devolatilization history of the particle yields the fraction of volatiles released in bed. The remaining volatiles are assumed to be released to freeboard while the particle is at the bed surface. With regard to combustion of volatiles released, volatile carbon and hydrogen are assumed to burn instantaneously to carbon monoxide (CO) and water (H_2O), respectively. The oxidation of CO takes place in both bubble and emulsion phases according to the rate expression of Hottel *et al.* [14].

2.2.3 Char Combustion

Both char particles originating from coal and biomass are assumed to burn only to CO, as it is the major product of char combustion for typical FBC temperatures. Using the shrinking particle model and taking film mass transfer and the kinetics

resistance into consideration, the rate of carbon oxidation at the particle surface can be obtained as:

$$r_{C,e} = \frac{2}{1/k_f + 2/k_s} \bar{C}_{O_2,e} \tag{2.12}$$

The film mass transfer coefficient, k_f, is obtained from the relation suggested by Jung and La Nauze [18]. In Eq. (2.12) average emulsion phase oxygen concentration is used to calculate combustion rate. Kinetics of combustion for lignite and biomass are assumed to be represented by the rate laws suggested by Field *et al.* [13] and Adanez *et al.* [12], respectively.

2.2.4 Char Particles Size Distribution

Total rate of char combustion is proportional to the char hold-up in the bed and external surface area of the char particles. From this point of view, the size distribution of char particles plays a key role for combustion systems. The size distribution is calculated based on population balance in every particle size intervals.

In this thesis study, char particle size distribution for lignite and biomass are determined separately by making population balance for each fuel. The steady state population balance on mass basis on char particles can be expressed as:

$$\left\{\begin{array}{c}\text{Char Entering}\\ \text{in feed}\end{array}\right\}_i + \left\{\begin{array}{c}\text{Char entering}\\ \text{in recycle}\end{array}\right\}_i - \left\{\begin{array}{c}\text{Char leaving}\\ \text{in bed drain}\end{array}\right\}_i - \left\{\begin{array}{c}\text{Char leaving}\\ \text{in carry over}\end{array}\right\}_i$$

$$+ \left\{\begin{array}{c}\text{Char shrinking into the}\\ \text{interval from a larger size}\end{array}\right\}_i - \left\{\begin{array}{c}\text{Char shrinking out of the}\\ \text{interval to a smaller size}\end{array}\right\}_i$$

$$- \left\{\begin{array}{c}\text{Char depleted within the}\\ \text{interval due to combustion}\end{array}\right\}_i + \left\{\begin{array}{c}\text{Char generated within the}\\ \text{interval due to attrition}\end{array}\right\}_i = 0 \tag{2.13}$$

where i represents the type of fuel: 1 for lignite, 2 for biomass. For the sake of clarity subscript i is removed in the following equations.

In order to drive an equation based on the mass fractions in size intervals for shrinking char particles the following assumptions are made:

1. Char particles enter the bed at a rate of F_0 with size distribution of $P_0(r)$ which is expressed by Rosin-Rammler size distribution function.

2. As char particles are well-mixed, bed drain char size distribution represents the bed char size distribution:

$$P_{bd}(r) = P_{bed}(r) \tag{2.14}$$

3. The rate of elutriation of char particles of size r is directly proportional to their concentration in the bed, i.e.,

$$F_{CO}P_{CO}dr = M_d P_{bed}(r)E(r)dr \tag{2.15}$$

   where $E(r)$ is the elutriation rate constant [20], M_d is the total mass of char in the bed and $P_{bed}(r)$ is the size distribution of char particles in the bed.

4. Carryover char size distribution represents the recycle char size distribution, since both streams are elutriated from the bed:

$$P_{CO}(r) = P_{recy} \tag{2.16}$$

5. Densities of char particles do not change during the burn-out.

6. Char particles can be attrited until reaching the upper size limit of fines, r_j, and then becomes fine itself. Fines generated by attrition are not attritable themselves.

7. Char particles are considered to shrink by combustion and attrition according to shrinking particle model at a rate of

$$\left(\frac{dr}{dt}\right) = \left(\frac{dr}{dt}\right)_c + U_f\left(r_{\max}, r_f\right)\left(\frac{dr}{dt}\right)_a \tag{2.17}$$

where U_f is unit filter function defined to function defined to differentiate particle size ranges attained due to both combustion and attrition and due to combustion only. A detailed discussion on definition of unit filter function can be found elsewhere [33].

Based on these assumptions, the working form of the population balance can be expressed as:

$$\frac{dW(r)}{dr} = -W(r)\left[\frac{F_{bd}}{M_d \Re(r)} + \left(1 - \frac{F_{recy}}{F_{CO}}\right)\frac{E(r)}{\Re(r)} - \frac{3}{r}\right]$$

$$+F_o P_o(r) + U_f\left(r_f, 0\right) F_a P_f(r) \tag{2.18}$$

Eq. (2.18) should be solved for both coal and biomass to calculate the char hold-up of both species. Detailed derivation of Eq. (2.18) can be found elsewhere [34]. In Eq. (2.18) $W(r)$ and $\Re(r)$ are defined as:

$$W(r) = M_d P_{bed}(r)\Re(r) \tag{2.19a}$$

$$\Re(r) = -\frac{dr}{dt} \tag{2.19b}$$

Equation (2.18) is subjected to boundary condition:

$$@ \quad r = r_{max} \qquad W(r) = 0 \tag{2.20}$$

Once solution of $W(r)$ becomes available, the bed char hold-up, M_d, bed char size distribution, $P_{bed}(r)$, carryover rate, F_{CO}, and carryover char size distribution,

$P_{CO}(r)$, can be calculated by following equations:

$$M_d = \int_{r_{min}}^{r_{max}} W(r)dr \tag{2.21a}$$

$$P_{bed}(r) = \frac{W(r)}{M_d \Re(r)} \tag{2.21b}$$

$$F_{CO} = \int_{r_{min}}^{r_{max}} M_d P_{bed}(r) E(r)dr \tag{2.21c}$$

$$P_{CO}(r) = \frac{M_d P_{bed}(r) E(r)}{F_{CO}} \tag{2.21d}$$

2.2.5 Desulfurization Model

It is assumed that desulfurization involves two consecutive steps, instantaneous calcination of limestone followed by sulfation reaction. This reaction is followed by the sulfation reaction. The sulfation reaction is assumed to be proportional to the external surface area lime which decreases with time due to pore blocking. The rate law for this equation may be written as:

$$r_{SO_2} = kC_{SO_2}S(t) \tag{2.22}$$

In Eq. (2.22) the $S(t)$ is the reactive external surface area of lime particles at a particle radius of r which is given in terms of fractional external surface area,$\sigma(t)$, in Eq. (2.23).

$$\frac{S(t)}{S_0} = \sigma(t) = \exp\left[- \frac{6\mathrm{M}_{\mathrm{CaCO_3}}\mathrm{kC}_{\mathrm{SO_2}}}{\mathrm{x}_{\mathrm{CaCO_3}}\rho_{lst}d_p}t \right] \tag{2.23}$$

where total initial external surface area for spherical limestone particles, S_0, is expressed as:

$$S_0 = \frac{6M_{lst}}{\rho_s d_p} \tag{2.24}$$

In order model sulfation reaction at steady state it is necessary to obtain an average fraction of external surface area, σ_{avg}, which can be obtained from solids residence time distribution function and the fractional external surface area as a function of time,

$$\begin{aligned}\sigma_{avg} &= \frac{1}{\left[1+\frac{6M_{CaCO_3}kC_{SO_2}}{x_{CaCO_3}\rho_{lst}d_p}\tau\right]} \\ &\times\left[1-\exp\left\{-\left(\frac{1}{\tau}+\frac{6M_{CaCO_3}kC_{SO_2}}{x_{CaCO_3}\rho_{lst}d_p}\right)\tau_{max}\right\}\right]\end{aligned} \tag{2.25}$$

Details of average external surface area calculation is given in detail elsewhere [34]. The final form of rate of sulfation reaction becomes,

$$r_{SO_2} = kC_{SO_2}S_0\sigma_{avg} \tag{2.26}$$

Then the total reaction rate is the summation of the rates obtained at different sizes:

$$r_{SO_2} = \sum_{i=1}^{n} r_{SO_2,i} \tag{2.27}$$

2.2.6 *NO* Formation and Reduction Model

It is generally accepted that nitrogen retained in char oxidizes to NO proportionally to char combustion rate. Rate of nitrogen removal from the char surface is assumed to be equal to the rate of oxidation at the particle surface, $r_{N,e}$. Therefore, for any char particle of size r, the rate of char nitrogen oxidation in the bed section, $n_{c,e}$, can be obtained in terms of char combustion rate, $n_{c,e}$ as given in Eq. (2.28). Details of the derivation can be found elsewhere [11].

$$n_{N,e} = \frac{(x_{N,c}/M_N)}{(x_C/M_C)} n_{C,e} \tag{2.28}$$

The related rate expressions for homogeneous and heterogeneous *NO* formation-reduction reactions are summarized in Table 2.1. The rate of heterogeneous reactions for all particles at any size r is the sum of individual reactions, r_{NO} on a single solid

particle. Reactions $R12$ and $R13$ have Arrhenius type of rate expressions including char particle temperature, T_d, so considering any char particle of size r, rate of heterogeneous reaction, r_{NO} equals to:

$$r_{N,het} = M_d \int_{r_{\min}}^{r_{\max}} P(r) r_{NO}\, dr \tag{2.29}$$

However, for reactions $R14$ and $R16$, the rate of heterogeneous reaction can be found by multiplying r_{NO} with char hold-up, M_d, directly,

$$r_{N,het} = M_d r_{NO} \tag{2.30}$$

and for reactions $R14$ and $R16$ with ash hold-up, M_i.

$$r_{N,het} = M_i r_{NO} \tag{2.31}$$

2.2.7 Mass and Energy Balance Equations

Spatial variations of species concentrations are described by the conservation equations for chemical species in bubble and emulsion phases:

$$\frac{dn_{j,b}}{dz} = A_{bed}\delta\left[\Re_{j,b} + K_{be}(C_{j,e} - C_{j,b})\right] \tag{2.32}$$

$$0 = n_{j,e}|_{z=0} - n_{j,e} + V_{bed}\delta\left[\frac{1-\delta}{\delta}\varepsilon_{mf}\Re_{j,e} - K_{be}(C_{j,e} - \bar{C}_{j,b})\right] \tag{2.33}$$

These equations are subject to the following boundary conditions:

$$\begin{aligned} @z = 0 \qquad n_{j,b} &= y_{j,b}\frac{n_a}{1 + \frac{u_e}{u_b}\frac{1-\delta}{\delta}\varepsilon_{mf}} \\ @z = 0 \qquad n_{j,e} &= y_{j,e}\frac{n_a}{1 + \frac{u_b}{u_e}\frac{\delta}{(1-\delta)\varepsilon_{mf}}} \end{aligned} \tag{2.34}$$

The expressions for the species generation or depletion terms appearing in Equations (2.33) and (2.32), $\Re_{j,b}$ and $\Re_{j,e}$, take the following forms for each species considered, $j = 1\,(O_2)$

$$\Re_{1,b} = -0.5 r_{CO,b} - \frac{5}{4}\left(r_{N,hom}\right)_{R10} \tag{2.35}$$

$$\begin{aligned}
\Re_{1,e} = & -\frac{m_{vmcoal} x_{vlcoal}}{V_{bed}(1-\delta)\varepsilon_{mf}} \left\{ 0.5\frac{x_{C,vm}}{M_C} + 0.5\frac{x_{H,vm}}{M_{H_2}} + \frac{x_{S,vm}}{M_S} - \frac{x_{O,vm}}{M_{O_2}} \right\}_{coal} \\
& -\frac{m_{vmbio} x_{vlbio}}{V_{bed}(1-\delta)\varepsilon_{mf}} \left\{ 0.5\frac{x_{C,vm}}{M_C} + 0.5\frac{x_{H,vm}}{M_{H_2}} + \frac{x_{S,vm}}{M_S} - \frac{x_{O,vm}}{M_{O_2}} \right\}_{bio} \\
& -0.5\left(n_{C,e_{coal}} + n_{C,e_{bio}}\right) - 0.5 r_{CO,e} - \frac{0.5 r_{SO_2,e}}{V_{bed}(1-\delta)\varepsilon_{mf}} \\
& -0.5 n_{N,e} - \frac{5}{4}\left(r_{N,hom}\right)_{R10} \\
& -\frac{1}{V_{bed}(1-\delta)\varepsilon_{mf}} \left\{ \begin{array}{l} \frac{5}{4}\left(r_{N,het}\right)_{R14} + \frac{5}{4}\left(r_{N,het}\right)_{R15} \\ +\frac{3}{4}\left(r_{N,het}\right)_{R16} + \frac{3}{4}\left(r_{N,het}\right)_{R17} \end{array} \right\}_{coal} \\
& -\frac{1}{V_{bed}(1-\delta)\varepsilon_{mf}} \left\{ \begin{array}{l} \frac{5}{4}\left(r_{N,het}\right)_{R14} + \frac{5}{4}\left(r_{N,het}\right)_{R15} \\ +\frac{3}{4}\left(r_{N,het}\right)_{R16} + \frac{3}{4}\left(r_{N,het}\right)_{R17} \end{array} \right\}_{bio}
\end{aligned} \tag{2.36}$$

$j = 2\,(CO)$

$$\Re_{2,b} = -r_{CO,b} \tag{2.37}$$

$$\begin{aligned}
\Re_{2,e} = & \frac{m_{vmcoal} x_{vlcoal}}{V_{bed}(1-\delta)\varepsilon_{mf}} \left\{ 0.5\frac{x_{C,vm}}{M_C} \right\}_{coal} + n_{C,e_{coal}} \\
& +\frac{m_{vmbio} x_{vl}bio}{V_{bed}(1-\delta)\varepsilon_{mf}} \left\{ 0.5\frac{x_{C,vm}}{M_C} \right\}_{bio} + n_{C,e_{bio}} - r_{CO,e} \\
& +\frac{1}{V_{bed}(1-\delta)\varepsilon_{mf}} \left\{ \left(r_{N,het}\right)_{R12} - \left(r_{N,het}\right)_{R13} \right\}_{coal} \\
& +\frac{1}{V_{bed}(1-\delta)\varepsilon_{mf}} \left\{ \left(r_{N,het}\right)_{R12} - \left(r_{N,het}\right)_{R13} \right\}_{bio}
\end{aligned} \tag{2.38}$$

$j = 3\,(CO_2)$

$$\Re_{3,b} = r_{CO,b} \tag{2.39}$$

$$\begin{aligned}\Re_{3,e} &= \frac{1}{V_{bed}(1-\delta)\varepsilon_{mf}}\left\{\left(r_{N,het}\right)_{R13}\right\}_{coal} \\ &+\frac{1}{V_{bed}(1-\delta)\varepsilon_{mf}}\left\{\left(r_{N,het}\right)_{R13}\right\}_{bio} \\ &+r_{CO,e}+\frac{F_{lst}x_{CaCO_3}}{M_{CaCO_3}V_{bed}(1-\delta)\varepsilon_{mf}}\end{aligned} \tag{2.40}$$

$j = 4\,(H_2O)$

$$\Re_{4,b} = \frac{3}{2}(r_{N,hom})_{R10}+\frac{1}{V_{bed}\delta}(r_{N,hom})_{R11} \tag{2.41}$$

$$\begin{aligned}\Re_{4,e} &= \frac{1}{V_{bed}(1-\delta)\varepsilon_{mf}}\left\{m_{vmcoal}x_{vlcoal}\frac{x_{H,vm}}{M_{H_2}}+m_f\frac{x_{H_2O}}{M_{H_2O}}\right\}_{coal} \\ &+\frac{1}{V_{bed}(1-\delta)\varepsilon_{mf}}\left\{m_{vmbio}x_{vlbio}\frac{x_{H,vm}}{M_{H_2}}+m_f\frac{x_{H_2O}}{M_{H_2O}}\right\}_{bio} \\ &-\frac{1}{V_{bed}(1-\delta)\varepsilon_{mf}}\left(r_{N,hom}\right)_{R11} \\ &+\frac{3}{2}\frac{1}{V_{bed}(1-\delta)\varepsilon_{mf}}\left\{\left(r_{N,het}\right)_{R14}+\left(r_{N,het}\right)_{R16}\right\}_{coal} \\ &+\frac{3}{2}\frac{1}{V_{bed}(1-\delta)\varepsilon_{mf}}\left\{\left(r_{N,het}\right)_{R14}+\left(r_{N,het}\right)_{R16}\right\}_{bio}\end{aligned} \tag{2.42}$$

$j = 5\,(SO_2)$

$$\Re_{5,b} = 0 \tag{2.43}$$

$$\Re_{5,e} = \frac{1}{V_{bed}(1-\delta)\varepsilon_{mf}}\left\{\begin{array}{c}\dfrac{m_{vmcoal}x_{vlcoal}x_{S,vm_{coal}}}{M_S} \\ +\dfrac{m_{vmbio}x_{vlbio}x_{S,vm_{bio}}}{M_S} \\ -r_{SO_2,e}\end{array}\right\} \tag{2.44}$$

$j = 6\,(NH_3)$

$$\Re_{6,b} = -(r_{N,hom})_{R10} - \frac{2}{3}\frac{1}{V_{bed}\delta}(r_{N,hom})_{R11} \tag{2.45}$$

$[10pt]$

$$\begin{aligned}\Re_{6,e} = {} & \frac{1}{V_{bed}(1-\delta)\varepsilon_{mf}}\left\{\frac{m_{vmcoal}x_{vlcoal}x_{N,vm_{coal}}}{M_N} + \frac{m_{vmbio}x_{vlbio}x_{N,vm_{bio}}}{M_N}\right\} \\ & + \frac{1}{V_{bed}(1-\delta)\varepsilon_{mf}}(r_{N,hom})_{R11} - \left(r_{N,hom}\right)_{R10} \\ & + \frac{1}{V_{bed}(1-\delta)\varepsilon_{mf}}\left\{-\left((r_{N,het})_{R16}\right)_{coal} - \left((r_{N,het})_{R16}\right)_{bio}\right\} \\ & + \frac{1}{V_{bed}(1-\delta)\varepsilon_{mf}}\left\{-(r_{N,het})_{R17}\right\}\end{aligned} \tag{2.46}$$

$j = 7\,(NO)$

$$\Re_{7,b} = -(r_{N,hom})_{R10} - \frac{1}{V_{bed}\delta}(r_{N,hom})_{R11} \tag{2.47}$$

$$\begin{aligned}\Re_{7,e} = {} & n_{N,e} + \left(r_{N,hom}\right)_{\mathrm{R10}} - \frac{1}{V_{bed}(1-\delta)\varepsilon_{mf}}\left(r_{N,hom}\right)_{R11} \\ & + \frac{1}{V_{bed}(1-\delta)\varepsilon_{mf}}\left\{\begin{array}{c}-\left(r_{N,het}\right)_{R12} - \left(r_{N,het}\right)_{R13} \\ [10pt] + \left(r_{N,het}\right)_{R14}\end{array}\right\}_{coal} \\ & + \frac{1}{V_{bed}(1-\delta)\varepsilon_{mf}}\left\{\begin{array}{c}-\left(r_{N,het}\right)_{R12} - \left(r_{N,het}\right)_{R13} \\ + \left(r_{N,het}\right)_{R14}\end{array}\right\}_{bio}\end{aligned} \tag{2.48}$$

On the assumption that the gas and the inert particles are at the same temperature and that the mass of combustion gases and char particles are negligible compared to the mass of inerts, a combined gas/solid phase energy balance can be written as,

$$
\begin{aligned}
0 \;=\;& Q_{rxn} + Q_p - m_f x_w \lambda^0 - n_g \sum_{j=1}^{8} y_j \int_{T_r}^{T_{bed}} c_{pg,j} dT \\
& - m_{recy} c_{pi} (T_{bed} - T_{recy}) - m_{co} c_{pi} (T_{bed} - T_r) \\
& - m_{bd} c_{pi} (T_{bed} - T_r) - A_{bw} h_{bw} (T_{bed} - T_{bw,s}) \\
& + n_A \int_{T_r}^{T_A} c_{pA} dT - \alpha \frac{A_T}{L_T} \int_0^{L_T} U_{cw} (T_{bed} - T_{cw}) dx
\end{aligned} \tag{2.49}
$$

where enthalpy generated by chemical reactions, Q_{rxn}, and energy transferred from burning char particles, Q_p, are obtained from following equations,

$$
\begin{aligned}
Q_{rxn} \;=\;& m_{f\,coal} x_{vm\,coal} x_{vl\,coal} \left\{ \begin{array}{l} \dfrac{x_{C,vm}}{M_C} \Delta H^0_{R2} + \dfrac{x_{H,vm}}{M_{H_2}} \Delta H^0_{R4} \\ + \dfrac{x_{S,vm}}{M_S} \Delta H^0_{R5} + \dfrac{x_{N,vm}}{M_N} \Delta H^0_{R8} \end{array} \right\}_{coal} \\
& + m_{f\,bio} x_{vm\,bio} x_{vl\,bio} \left\{ \begin{array}{l} \dfrac{x_{C,vm}}{M_C} \Delta H^0_{R2} + \dfrac{x_{H,vm}}{M_{H_2}} \Delta H^0_{R4} \\ + \dfrac{x_{S,vm}}{M_S} \Delta H^0_{R5} + \dfrac{x_{N,vm}}{M_N} \Delta H^0_{R8} \end{array} \right\}_{bio} \\
& + \Delta H^0_{R3} \int_0^{H_{bed}} r_{CO,b} dz + \Delta H^0_{R10} \int_0^{H_{bed}} \left(r_{N,\mathrm{hom}} \right)_{R10,b} dz \\
& + \frac{\Delta H^0_{R11}}{V_{bed} \delta} \int_0^{H_{bed}} \left(r_{N,\mathrm{hom}} \right)_{R11,b} dz - \frac{F_{lst} x_{CaCO_3}}{M_{CaCO_3}} \Delta H^0_{R6} \\
& + V_{bed} (1 - \delta) \varepsilon_{mf} \left\{ \Delta H^0_{R3} r_{CO,e} + \Delta H^0_{R10} \left(r_{N,\mathrm{hom}} \right)_{R10,e} \right\}
\end{aligned}
$$

$$
\begin{aligned}
&+V_{bed}(1-\delta)\varepsilon_{mf}\left\{\Delta H^0_{R9}\left\{n_{N,e_{coal}}+n_{N,e_{bio}}\right\}\right\}+\Delta H^0_{R11}\left(r_{N,\mathrm{hom}}\right)_{R11,e}\\
&+\left\{\begin{array}{l}\Delta H^0_{R12}\left(r_{N,het}\right)_{R12}+\Delta H^0_{R13}\left(r_{N,het}\right)_{R13}\\ +\Delta H^0_{R14}\left(r_{N,het}\right)_{R14}+\Delta H^0_{R16}\left(r_{N,het}\right)_{R16}\end{array}\right\}_{coal}\\
&+\left\{\begin{array}{l}\Delta H^0_{R12}\left(r_{N,het}\right)_{R12}+\Delta H^0_{R13}\left(r_{N,het}\right)_{R13}\\ +\Delta H^0_{R14}\left(r_{N,het}\right)_{R14}+\Delta H^0_{R16}\left(r_{N,het}\right)_{R16}\end{array}\right\}_{bio}\\
&+\Delta H^0_{R17}\left(r_{N,het}\right)_{R17}+\Delta H^0_{R15}\left(r_{N,het}\right)_{R15}
\end{aligned}
\tag{2.50}
$$

$$
Q_p = \frac{3M_d}{\rho_d}\int_{r_{\min}}^{r_{\max}}\left[h_p(T_d-T_{bed})+\sigma\varepsilon(T_d^4-T_{bed}^4)\right]\frac{dr}{r} \tag{2.51}
$$

Particle temperature in Eq. (2.51) is calculated by solving an energy balance around a single particle which is assumed to have uniform temperature:

$$
\frac{\rho_d}{M_C}\frac{x_{fc}}{x_{fc}+x_a}\Delta H^o_{R1}\Re(r)-\left\{h_p\left(T_d-T_{bed}\right)+\sigma\varepsilon\left(T_d^4-T_{bed}^4\right)\right\}=0 \tag{2.52}
$$

Energy loss through the bed walls is taken into account by making a one-dimensional heat transfer analysis. For a combustor with square cross-section and wall thickness of L_{bw}, the temperature profile inside the wall of variable cross section is given by the following equation:

$$
\frac{d^2T_{bw}}{dx^2}\left(x+A_{bed}^{0.5}/2\right)+\frac{dT_{bw}}{dx}=0 \tag{2.53}
$$

Equation 2.53 is subjected to the followig boundary conditions:

$$
\begin{aligned}
@x=0 \qquad & h_{bw}\left(T_{bed}-T_{bw}\right)= -k_{bw}\frac{\partial T_{bw}}{\partial x}\\
@x=L_{bw} \qquad & T_{bw}= T_{bw,o}
\end{aligned}
\tag{2.54}
$$

In order to account for the energy absorbed by the in-bed heat exchanger, a separate energy balance is performed on the cooling water. Neglecting the heat transfer

resistance of the tubes, the spatial variation of the temperature of the cooling water is given by the following equation:

$$\frac{4m_{cw}}{\pi}\frac{dT_{cw}}{dx} - \frac{4d_{T,o}}{c_{pcw}}h_{cw}\left(T_{bed} - T_w\right) = 0 \tag{2.55}$$

The inlet temperature of the cooling water is set as boundary condition to Equation 2.55. Surface temperature of tube wall, T_w, is calculated by solving a surface energy balance:

$$h_{cw}d_{T,o}\left(T_{bed} - T_w\right) - h_i d_{T,i}\left(T_w - T_{cw}\right) = 0 \tag{2.56}$$

2.3 Freeboard Model

2.3.1 Solids Distribution

The hold-up of particles in the freeboard is expressed with an exponential decay function of Choi *et al.* [20],

$$\frac{\varepsilon_s}{\varepsilon_{s,0}} = \exp\left(-az_f\right) \tag{2.57}$$

where $\varepsilon_{s,0}$ term is the volume fraction of solids just above the surface of dense bubbling bed and given by:

$$\varepsilon_{s,0} = 1 - \varepsilon_f \tag{2.58}$$

The volume fractions of char and inert particles of size r at bed surface are obtained from the following equations, respectively:

$$\varepsilon_{d,0} = \varepsilon_{s,0} \frac{M_d P_{bed}(r)\Delta r/\rho_d}{M_d/\rho_d + M_i/\rho_i} \tag{2.59}$$

$$\varepsilon_{i,0} = \varepsilon_{s,0} \frac{M_i P_{bed}(r)\Delta r/\rho_i}{M_d/\rho_d + M_i/\rho_i} \tag{2.60}$$

The entrainment flux of particles, K_i^*, is calculated by assuming that it consists of a cluster flux, K_{ih}^*, and a dispersed noncluster flux, $K_{i\infty}^*$ as suggested by Hazlett and Bergougnou [35],

$$K_i^* = K_{ih}^* + K_{i\infty}^* \tag{2.61}$$

and are obtained from empirical correlations proposed by Choi *et al.* [20]. The elutriation rate constant, E(r), defined in Eq. (2.15) is then calculated from:

$$E(r) = \frac{A_{bed}}{M_d} K^*_{i\infty} \tag{2.62}$$

The elutriated particles are assumed to rise at the superficial gas velocity in the freeboard. Size distribution of entrained solid particles at any height in the freeboard is calculated by assuming that probability of finding particles of size r at any height is proportional to their presence in bed with proportionality constant being K^*_{ih}:

$$F_z P_z(r) = K^*_{ih} A_{bed} P_{bed}(r) \tag{2.63}$$

Multiplying both sides of Equation 2.63 by dr and integrating yields the flow rate of entrained particles and their size distribution as follows:

$$F_z = A_{bed} \int_{r_{\min}}^{r_{\max}} K^*_{ih} P_{bed}(r) dr \tag{2.64}$$

$$P_z(r) = \frac{A_{bed} K^*_{ih} P_{bed}(r)}{F_z} \tag{2.65}$$

2.3.2 Mass and Energy Balance Equations

It is assumed that the gases in the bubble and emulsion phases mix instantaneously at the top of the bed and enter freeboard. The gas flow in freeboard is assumed to be in plug flow. A shell mass balance for j^{th} gas component in the freeboard results in the following equation:

$$\frac{dn_{j,f}}{dz} = A_f (1 - \varepsilon_s) \Re_{j,f} \tag{2.66}$$

Equation 2.66 is subjected to the following boundary condition:

$$@z_f = 0 \qquad n_{j,f} = n_{j,e} + n_{j,b} \tag{2.67}$$

For the species under consideration the species generation term, $\Re_{j,f}$, can be expressed as follows:

$j = 1\,(O_2)$

$$\begin{aligned}\Re_{1,f} &= -\frac{m_{vmcoal}\,(1-x_{vlcoal})}{V_f\,(1-\varepsilon_s)}\left\{0.5\frac{x_{C,vm}}{M_C}+0.5\frac{x_{H,vm}}{M_{H_2}}+\frac{x_{S,vm}}{M_S}-\frac{x_{O,vm}}{M_{O_2}}\right\}_{coal}\\ &\quad -0.5\left(n_{C,f\,coal}\right)\\ &\quad -\frac{0.5r_{SO_2,f}}{V_f\,(1-\varepsilon_s)}-0.5r_{CO,f}-\frac{5}{4}\left(r_{N,\mathrm{hom}}\right)_{R10}\end{aligned} \tag{2.68}$$

$j = 2\,(CO)$

$$\begin{aligned}\Re_{2,f} &= \frac{m_{vmcoal}\,(1-x_{vlcoal})}{V_f\,(1-\varepsilon_s)}\left\{0.5\frac{x_{C,vm}}{M_C}\right\}_{coal}+n_{C,f\,coal}\\ &\quad -r_{CO,f}\end{aligned} \tag{2.69}$$

$j = 3\,(CO_2)$

$$\Re_{3,f} = r_{CO,f} \tag{2.70}$$

$j = 4\,(H_2O)$

$$\begin{aligned}\Re_{4,f} &= \frac{1}{V_f\,(1-\varepsilon_s)}\left\{m_{vmcoal}\,(1-x_{vlcoal})\left(\frac{x_{H,vm}}{M_{H_2}}\right)_{coal}+\left(r_{N,hom}\right)_{R11}\right\}\\ &\quad +\left(r_{N,hom}\right)_{R10}\end{aligned} \tag{2.71}$$

$j = 5\,(SO_2)$

$$\Re_{5,f} = \frac{1}{V_f\,(1-\varepsilon_s)}\left\{m_{vmcoal}\,(1-x_{vlcoal})\left(\frac{x_{S,vm}}{M_S}\right)_{coal} - r_{SO_{2,f}}\right\} \tag{2.72}$$

$j = 6\,(NH_3)$

$$\begin{aligned}\Re_{6,f} \;=\; & \frac{1}{V_f\,(1-\varepsilon_s)}\left\{m_{vmcoal}\,(1-x_{vlcoal})\left(\frac{x_{N,vm}}{M_N}\right)_{coal} - \left(r_{N,hom}\right)_{R11}\right\} \\ & - \left(r_{N,hom}\right)_{R10}\end{aligned} \tag{2.73}$$

$j = 7\,(NO)$

$$\Re_{7,f} = \left\{\left(r_{N,\mathrm{hom}}\right)_{R10} - \frac{1}{V_f(1-\varepsilon_s)}\left(r_{N,\mathrm{hom}}\right)_{R11}\right\} \tag{2.74}$$

where $n_{C,f_{coal}}$, the solid carbon consumption rate at any height in freeboard is the sum of carbon consumption rates for coarse and fine particles, as shown below

$$n_{C,f} = -\frac{3\eta}{M_C}\frac{x_{fc}}{x_{fc}+x_a}\left\{\rho_d \int_{r_{\max e}}^{r_{\max}} \frac{\varepsilon_{s,d}P_z(r)}{r}\Re_f(r)dr + \frac{F_{co}}{A_f}\int_{r_{\min}}^{r_{\max}} \frac{P_{co}(r)}{ru_p(r)}\Re_f(r)dr\right\} \tag{2.75}$$

η in Equation (2.75) represents the contact efficiency between gas and solids in freeboard and it is calculated from the following equation proposed by Kunii and Levenspiel [21],

$$\eta = 1-(1-\eta_0)\exp\left(-6.62\,z_f\right) \tag{2.76}$$

where

$$\eta_0 = \frac{u_e}{u_0}\,(1-\delta) \tag{2.77}$$

The gas temperature profile in freeboard is obtained by solving an energy balance which considers convective transport and, generation and loss of energy:

$$\frac{dT_f}{dz} = \frac{A_f\left(1-\varepsilon_s\right)}{n_f c_{p,g}}\mathbf{R} \tag{2.78}$$

Equation (2.78) is subjected following boundary condition:

$$@\ z=0 \qquad T_f = T_{bed} \tag{2.79}$$

R in Eq. (2.78) is the combined energy generation and loss rate per unit volume of freeboard and defined as:

$$\mathbf{R} = \mathbf{R_{rxn}} + \mathbf{R_{fw}} + \mathbf{R_p} \tag{2.80}$$

$\mathbf{R_{rxn}}$, $\mathbf{R_{fw}}$ and $\mathbf{R_p}$ terms in Equation (2.80) are energy generated by chemical reactions, energy loss from freeboard walls and energy exchange between solid particles and the gaseous medium, respectively. These terms can be expressed as follows:

$$\begin{aligned}\mathbf{R_{rxn}} &= \frac{m_{vmcoal}\left(1-x_{vlcoal}\right)}{V_f\left(1-\varepsilon_s\right)}\left\{\begin{array}{l}\dfrac{x_{C,vm}}{M_C}\Delta H^0_{R2} + \dfrac{x_{H,vm}}{M_{H_2}}\Delta H^0_{R4} \\ +\dfrac{x_{S,vm}}{M_S}\Delta H^0_{R5} + \dfrac{x_{N,vm}}{M_N}\Delta H^0_{R8}\end{array}\right\}_{coal} \\ &\quad +\Delta H^0_{R3} r_{CO,f} + \frac{1}{V_f\left(1-\varepsilon_s\right)}\left[\Delta H^0_{R7} r_{SO_2,f} + \Delta H^0_{R11}\left(r_{N,het}\right)_{R11,f}\right] \end{aligned} \tag{2.81}$$

$$\mathbf{R_{fw}} = -\frac{4d_{bed}}{A_{bed}\left(1-\varepsilon_s\right)} h_{fw}\left(T_f - T_{fw}\right) \tag{2.82}$$

$$\mathbf{R_p} = \left\{ \begin{array}{l} \dfrac{3F_{co}}{A_{bed}\rho_d} \displaystyle\int_{r_{\min}}^{r_{\max e}} \dfrac{P_{z,d}(r)}{r\,u_p(r)} \left\{ h_p \left(T_d - T_f\right) + \sigma\varepsilon \left(T_d^4 - T_f^4\right) \right\} dr \\ +3\varepsilon_d \displaystyle\int_{r_{\max e}}^{r_{\max}} \dfrac{P_{z,d}(r)}{r} \left\{ h_p \left(T_d - T_f\right) + \sigma\varepsilon \left(T_d^4 - T_f^4\right) \right\} dr \end{array} \right\}_{coal}$$

$$+3\varepsilon_i \int_{r_{\max e}}^{r_{\max}} \frac{P_{z,i}(r)}{r} \left[h_p \left(T_i - T_f\right) + \sigma\varepsilon \left(T_i^4 - T_f^4\right) \right] dr \tag{2.83}$$

It is assumed that in freeboard char particles temperatures are equal to their temperatures in bed as calculated by Eq. (2.83) and temperatures of inert particles remain at T_{bed}. A surface energy balance is formulated to solve for temperature of freeboard wall,

$$h_f \left(T_f - T_{fw}\right) - \frac{\left(T_{fw} - T_{fw,o}\right)}{R_w} = 0 \tag{2.84}$$

where h_f is calculated by using the approach of Kunii and Levenspiel [21]:

$$\frac{h_f - (h_r + h_g)}{h_{zf=0} - (h_r + h_g)} = \exp\left(-a\, z_f / 2\right) \tag{2.85}$$

2.4 Solution Procedure

The input data required by the system model are the configuration of the rig and its internals, air, coal and biomass flow rates, coal and biomass analysis, all solid and gas properties, inlet temperatures of air, cooling water and feed solids and the size distribution function of feed solids deduced from sieve analysis.

Apart from these input data, application of the model necessitates empirical and semi-empirical correlations from the literature for heat and mass transfer, hydrodynamics related correlations etc., listed in Table 2.2. These expressions contain empirical or semi-empirical constants which may not always comply with the experimental conditions of the system to be modeled. Therefore, it is the

usual practice to adjust some of these constants until a compromise is found to reproduce the measured data as accurately as possible [36]. In this study, minimum number of fitting parameters was utilized. These were pre-exponential factor for carbon monoxide oxidation, exponential decay constant for entrained particles and elutriation rate constant.

CO concentrations predicted by using the rate expression of Hottel *et al.* [14] was found three orders of magnitude lower than the measurements. To match the measured *CO* concentration at the exit of the combustor, the rate constant from Hottel *et al.* was multiplied by 0.1 and this value was used for model validation. The effect of pre-exponental factor on *CO* concentration can be found in Appendix C.

Direct use of elutriation rate expression of Choi *et al.* [20] in the model yielded higher carryover flow rate at the cyclone exit. To match the measured carryover flow rates, elutriation rate constant of Choi *et al.* was multiplied by 0.022 for Run 1, 0.034 for Run 2 and 0.064 for Run 5. Fine-tuning for the carryover flow rates at the cyclone exit was the simplest approach as the carryover flow rate was only a function of elutriation.

The solution starts with making initial guesses for T_{bed}, $\bar{y}_{O_2,e}$, M_{dcoal}, M_{dbio}, F_a, $T_{bw,o}$, f_{3bio}/f_3. This is followed by computation of $\overline{T}_d$ by using estimated parameters. There are seven loops of iterations to be converged for M_{dcoal}, M_{dbio}, F_a, $\bar{y}_{O_2,e}$, $\overline{T}_{dcoal}$, $\overline{T}_{dbio}$, T_{bed}.

For each loop, a convergence criterion, ε, is set as the absolute difference between calculated and estimated values of the parameters. The predictions reported in this study were obtained with values of 1, 1, 1, 1×10^{-3}, 1×10^{-3}, 1×10^{-3} and 5×10^{-3}, 0.025 for iterations on T_{bed}, $\overline{T}_{dc}oal$, $\overline{T}_{db}io$, $\bar{y}_{O_2,e}$, M_{dcoal}, M_{dbio}, F_a, f_{3bio}/f_3, respectively. Figure 2.3 to Figure 2.5 shows the algorithm of the steady state model code in compact form.

The integration of ODEs is carried out by Backward-Differentiation Formula (BDF) method embedded in the ODE solver LSODES [37]. Solution of the non-linear

algebraic equations is performed by using the subroutine ZERO. Details of the solution procedure of steady state code for coal combustion can be found in [38].

The total CPU time for the complete model is about 70 seconds on 2.4 GHz Intel Pentium IV computer.

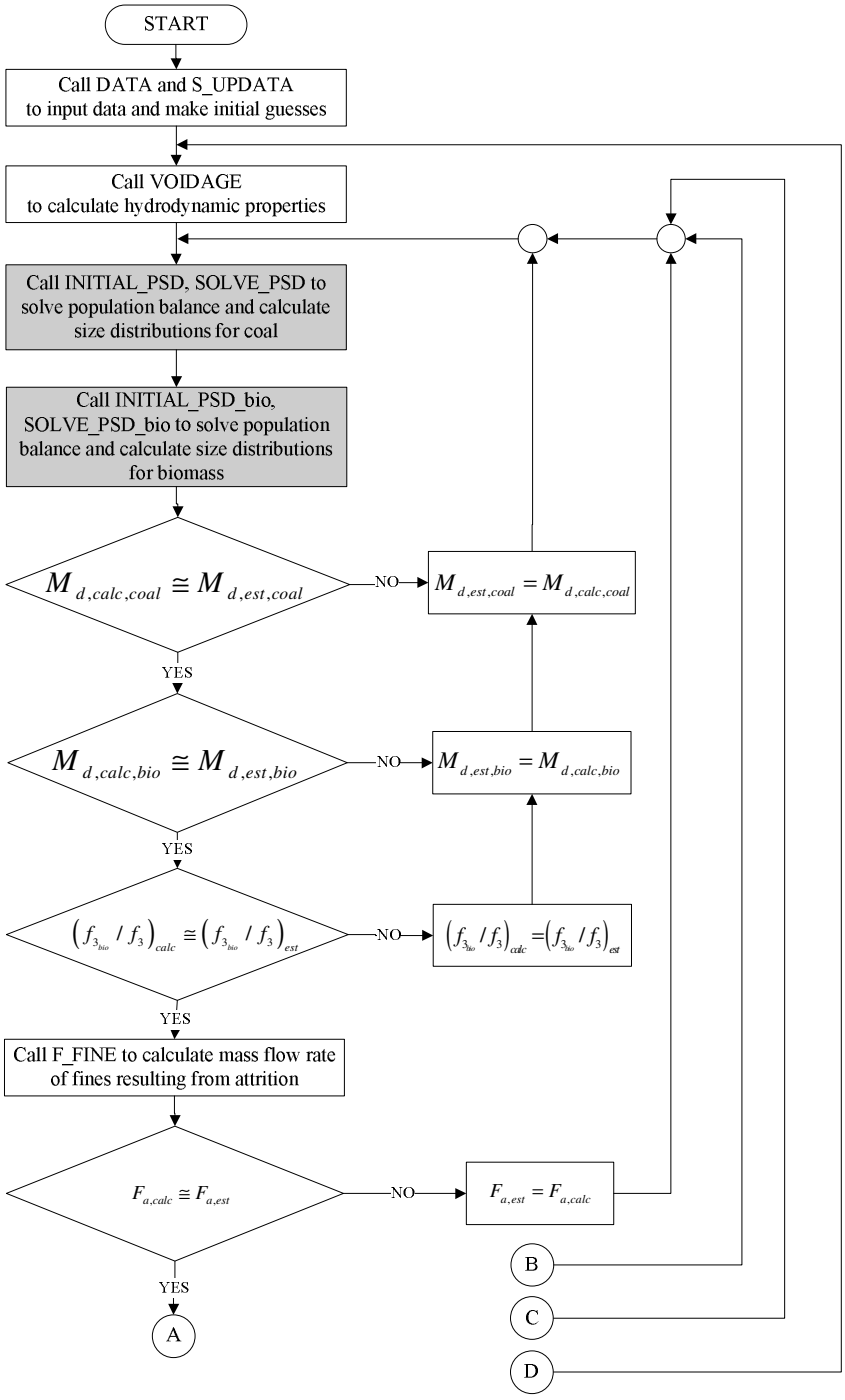

Figure 2.3: Algorithm for steady state code showing modified sections in this study in shade.

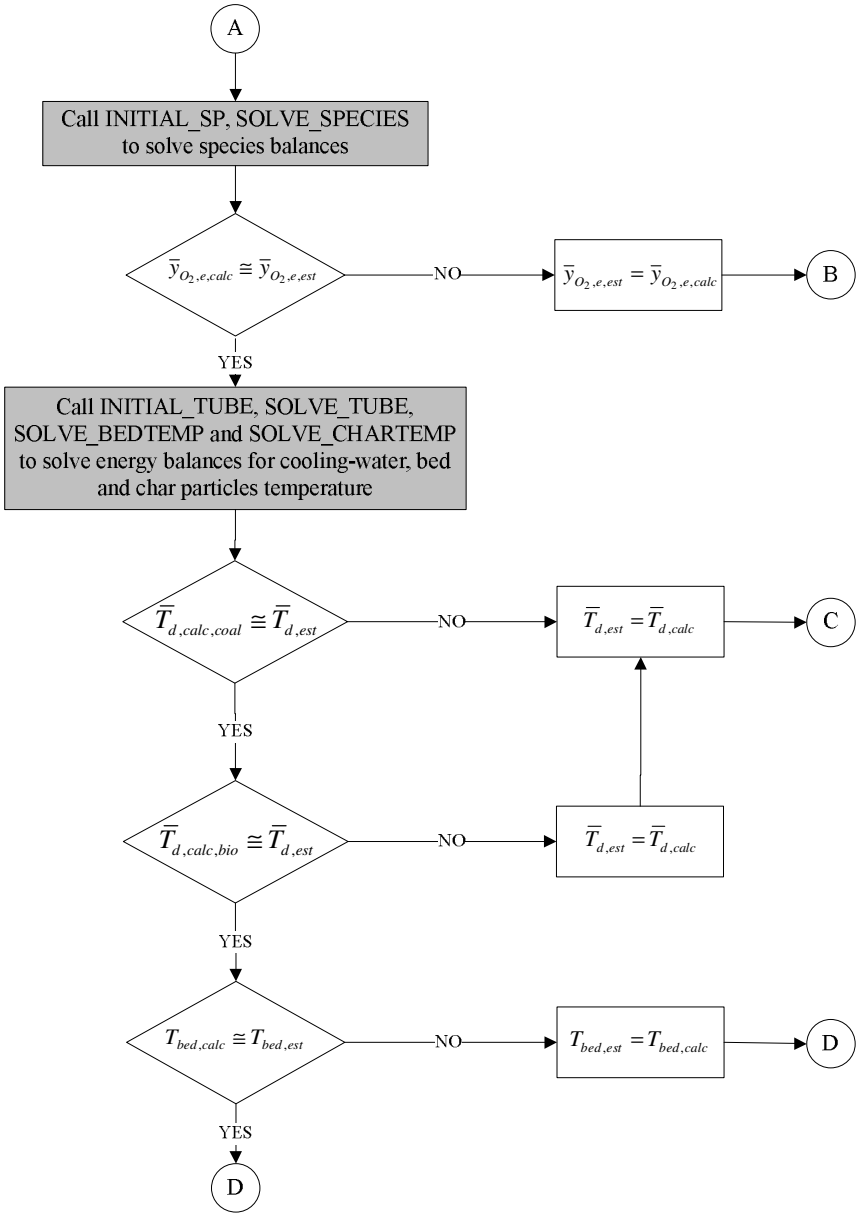

Figure 2.4: Algorithm for steady state code showing modified sections in this study in shade.

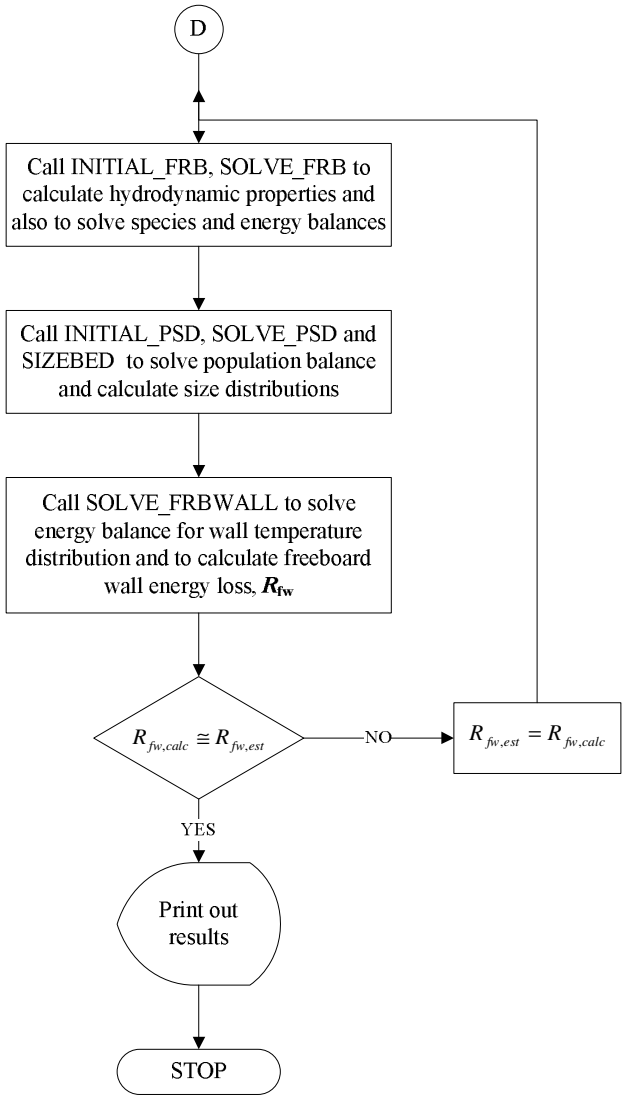

Figure 2.5: Algorithm for steady state code showing modified sections in this study in shade .

CHAPTER 3

EXPERIMENTAL SET-UP AND CONDITIONS

3.1 0.3 MWt ABFBC Test Rig

Experimental work was carried out on a 0.3 MWt ABFBC Test Rig designed and constructed within the scope of a cooperation agreement between Middle East Technical University (METU), Babcock & Wilcox GAMA (BWG) under the auspices of Canadian Development Agency (CIDA) for the investigation of combustion and in-situ desulfurization characteristics of low quality Turkish lignites. The existing test rig was extended to incorporate a baghouse filter for capture of fine fly ash leaving with the flue gas through the stack within the scope of a recent research project, MİSAG-159, financed by The Scientific and Technical Research Council of Turkey (TÜBİTAK). The test rig in its present form is shown schematically in Figure 3.1 below. As can be seen from the figure, the test rig basically consists of a forced draft (FD) fan, a windbox with an ash removal system, a modular combustor, a cyclone with a recycle leg, a baghouse filter, an induced draft (ID) fan and a coal and limestone feeding system.

3.1.1 The Combustor

The main body of the test rig is the modular combustor formed by five modules of equal dimensions. Each module has an internal cross-section of 0.45 m x 0.45 m and height of 1 m. Inner walls of each module are refractory lined with firebricks with a thickness of 6 cm. Outer walls of the refractory bricks are insulated with insulation bricks with thickness of 20 cm. Further insulation is provided by leaving an air gap of 6 mm between the outer wall of insulation brick and the inner wall of the steel construction of each module.

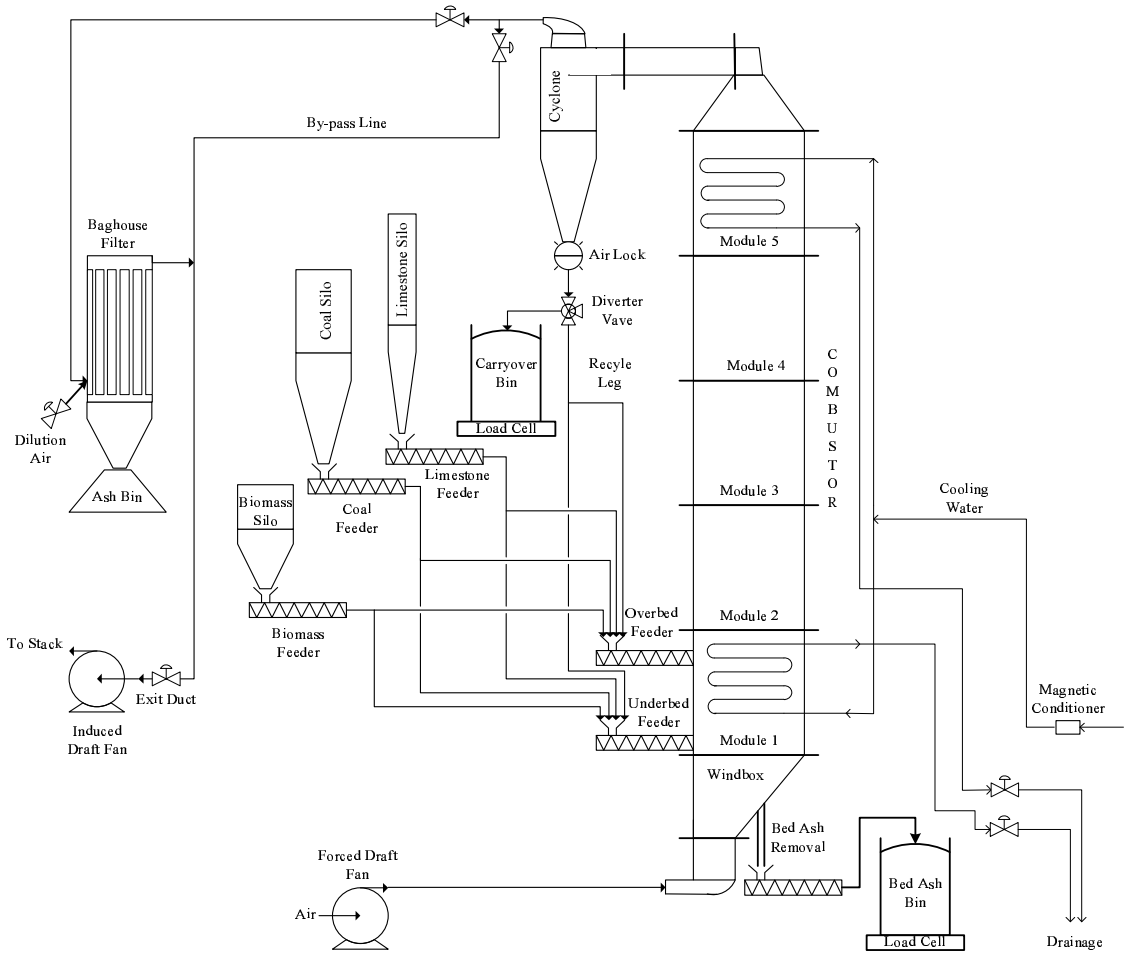

Figure 3.1: Schematic representation of METU 0.3 MW test rig.

The first and fifth modules from the bottom are referred as bed and cooler, respectively, and the ones in between are referred as freeboard modules. The bed module provides an expanded bed height of 1 *m*. It contains 6 water-cooled U-tubes (25 *mm* OD, stainless steel) for cooling purposes, 5 ports for thermocouples, 6 ports for gas sampling probes, one port for LPG distributor, one port for the ignitor and two ports for feeding fuel/limestone mixture. One of the feeding ports is 22 *cm* and the other is 85 *cm* above the distributor plate. There are 6 ports for gas sampling probes and 9 ports for thermocouples in freeboard and cooler modules. There exists a water-cooled tube bundle consisting of 11 tubes (26.7 *mm* OD, carbon steel) with 14 passes installed across the cross-section of the cooler module for cooling the stack gases before leaving the combustor.

3.1.2 Air and Gas System

The fluidizing air fed by the FD fan enters the bottom of the windbox through a pipe of 6.5 *m* long and 7.8 cm ID on which a manual gate valve, an automatic butterfly valve and a vortex flowmeter are installed. The design of the windbox allows the installation of bed ash removal system as shown in Figure 3.1. It is a mobile windbox supported by four wheels and a distributor plate is placed on the top. Air supplied to the windbox by means of the pipe of 7.8 *cm* ID diverges to the full cross-section of the combustor at the distributor plate located 1.4 *m* above the entrance port. Sieve type distributor plate contains 412 holes, each 4.5 *mm* in diameter, arranged in a triangular pattern. Within the bed module air mixes with fuel and limestone to affect combustion and sulfur capture.

Flue gases and elutriated fines leaving the bed surface enter the freeboard. Sufficient freeboard height is provided to permit burnout of elutriated char fines and combustible gases.

After leaving the freeboard, flue gases pass through the cooler module to cool the hot combustion gases. Flue gases leaving the modular combustor enter the cyclone and then the baghouse filter to leave the elutriated particles before passing through ID

fan to exit from the stack. As the temperature of the flue gases entering the baghouse filter is limited by the maximum operating temperature of the bag material which is 260 °C for the bag material (P84-Polyimide) selected for the baghouse filter under consideration, two alternative systems were provided for the safe operation of the baghouse filter: A bypass line between the cyclone and the ID fan and an air dilution system to reduce the flue gas temperature at the inlet to the filter through a slide valve if the temperature exceeds the upper operating limit of the bag material, 490 K.

The pipes carrying the flue gases before and after the baghouse filter are 14.0 and 5.3 *m* long, respectively, and have an ID of 15.3 *cm*. The pipeline between the cyclone and the ID fan of the existing test rig before the incorporation of baghouse filter was used as the bypass line. It has an ID of 12.8 *cm* and length of 14.5 *m*. The outlet of the baghouse filter joins this pipeline 4.2 *m* before the ID fan.

An orifice meter with a bore diameter of 8.05 *cm* was installed at the stack gas line before ID fan to measure the flow rate of the flue gases. The pressure drop across the orificemeter is measured by means of pressure transmitter. Knowing the temperature and pressure of the flue gases passing through the orificemeter, the signal from the transmitter is interpreted in the control system to yield molar flow rate.

3.1.3 Solids Handling System

Lignite, biomass and limestone are stored in three separate silos and conveyed into the hoppers of feeders at controlled flow rates via precalibrated volumetric feeders placed under their respective silos. Feeding of the mixture is so arranged that it is possible to feed the system either through the inbed feeding system (85 *cm* above the distributor plate) or the underbed feeding system (22 cm above the distributor plate).

Bed ash is withdrawn from the bed through 5 *cm* ID, 1.1 *m* long water-cooled ash removal pipe. Some of the bed ash is disposed and the rest is stored to provide bed inventory when required. Bed ash drain rate is adjusted from the computer to obtain the desired bed pressure drop and hence the expanded bed height. Bed ash particles

are collected in a continuously weighted ash storage bin.

The majority of the elutriable fines produced from solid in the bed and those fed within the solid streams are captured by the cyclone. Particles caught in the cyclone pass through an air lock (i.e. a rotary valve) and fall onto a diverter. Depending on the position of the diverter, particles are either discharged from the system to a continuously weighted ash storage bin for experiments without recycle or recycled to the combustor for refiring.

In order to catch fine particles of fly ash ($d_p < 40\,\mu m$) leaving the cyclone, a pulse-jet type baghouse filter with a 100 % collection efficiency for particles greater than 1 μm was utilized.

Before putting the baghouse filter into service, a permanent pre-coat is formed on the outer surface of the bags in order to increase the collection efficiency solely provided by the porosity of the bag material itself. This is accomplished by passing the fine CaO particles through the filter. During the service, an additional filter cake is built up at the outer surface of the bags which in turn becomes a principal collection medium. As the filter cake gets thicker with time, a pulse of compressed air is directed into the bag from the open top, which causes a shock wave to travel down its length dislodging the filter cake from the outer surface of the bag. A unique aspect of the pulse jet system is the use of a wire cage in each bag to keep it from collapsing during normal filtration. The bag hangs from the tube sheet. A series of parallel pulse jet pipes are located above the bags with each pipe row having a solenoid valve. This allows the bags to be pulsed clean one row of five bags at a time. Filter cake cleaned off the surface fall into a hopper and is discharged to fly ash collecting container. There are two containers each having a volume of 0.13 m^3. During filtration of flue gases if one container gets full, the maximum level device gives alarm by lighting the level warning light located on control panel, and the container full of ash is replaced with the other one after closing the ash discharge opening by leak proof slide valve.

3.1.4 Cooling Water System

Cooling water required for the test rig is passed through a magnetic conditioner and is then divided into two streams, one for the in-bed tube bundles, the other for the tube bundle in the cooler module. Heat transfer areas provided by the bed and cooler modules are 0.30 m^2 and 4.3 m^2, respectively. The cooling water in bed enters lower header and leaves the bed through the upper header. The cooling water for the cooler module enters the upper header and flows downward to provide counter-current flow to the up flowing flue gases. Water flow rates are adjusted by means of either a manual or a pneumatic control valve located at the drain of each stream to maintain maximum exit temperature of about 60 °C.

3.1.5 Gas Sampling System

Benefits of using advanced analytical instrumentation are negated unless a representative sample from the point of extraction can be obtained. Areas of concern in continuous gas sampling pointed out in detail by Anthony *et al.* [39] can be summarized as follows:

1. A sample must be subjected to minimum thermal chemical or fluid-mechanical disturbances by the sampling system. It is necessary to quench gas phase reactions at the point of sampling particularly when analyzing for minor constituents such as NO_x and CO.

2. The sample must be conditioned and transported to the analyzers without changing the concentration ratios of components to be measured. Conditioning is essential as the analyzers are designed to operate at near ambient temperatures and pressures and with dry, particulate free, non-corrosive, non-interfering samples. Therefore, particular care must be taken in gas sample cleanup to remove the particulates that are characteristic of Atmospheric Fluidized Bed Combustors (AFBC) and to remove the excess moisture that might otherwise condense in the sampling lines or analyzer banks. Another problem is that gaseous species may be partly lost along

the transport line because of homogeneous or catalytic reactions or simply by absorption of gas phase species such as SO_2 in the condensate is another possible source of error, while subsequent desorption can lead to erroneously high values when sampling lower concentrations.

3. In order to accurately measure the species of interest the analyzers must also be properly calibrated and maintained.

4. The sample extraction system must be durable because of the high-temperature, corrosive atmosphere present in the combustor.

Once through the probe, the sampled combustion gas is passed through a solenoid valve and sent to the gas conditioning and analysis system of the test rig by means of sample line. The sample line itself is maintained at 150 °C by means of a variable DC power supply so that no water, sulfuric acid or hydrocarbons would condense along the sampling interface. In addition, all lines and fittings in contact with the gas sample are made of teflon or stainless steel to prevent interferences due to gas adsorption or heterogeneous reactions. The existing analytical system of the test rig consists of a bank of analyzers for O_2, CO, CO_2, SO_2 and NO/N_2O. The positions of the gas sampling probes are given in Table 3.1. Gas is sampled at a rate of 13 cm^3/s at STP which is small enough to cause minimal interference to the combustion system. After passing through the probe, sample gas is transported through the heated stainless steel line to gas drier. Once through the drier, the gas is cooled, filtered and pumped to the analyzers via a teflon-coated diaphragm-type sample pump. Then, sample gas is let to flow through set of analyzers in series. After the measurement of species concentrations, sample gas is vented to the atmosphere. On-line wet analyses of O_2 and CO are also carried out at the exit of the combustor.

Table 3.1: Relative positions of gas sampling probes.

Probe No	**Distance above the distributor plate,** *cm*
P10	26
P9	56
P8	69
P7	85
P6	123
P5	183
P4	291
P3	344
P2	419
P1	500

3.2 Instrumentation and Analytical Systems

Instrumentation and analytical systems can be divided into following categories:

- Data acquisition and control system
- Solid flow control and monitoring
- Air and gas flow control and monitoring
- Cooling-water flow control and monitoring
- On-line continuous gas analyzers
- Pressure sensors
- Temperature sensors
- Solids analysis

The test rig is equipped with a data acquisition and control system namely Bailey INFI 90. Real time process data is monitored, manipulated, collected and analyzed with the aid of a control software called Bailey LAN-90 Process Control View installed on an IBM compatible PC 486 computer running under QNX operating system. The control system scans the signals coming from all of the instruments attached to it in a fraction of a second and reports and logs their averages discretely for 30 seconds of intervals. An uninterruptible power supply is connected to Bailey INFI 90 and PC in order to enable proper shut-down in case of a electricity cut-off by preventing corruption of data logged.

Fuel and sorbent feed rates are controlled manually by adjusting the fuel feeder or sorbent feeder control dial from the computer. The flow rates of fuel and sorbent are normally set to such values that provide desired excess air and Ca/S molar ratio, respectively. Bed ash drain rate can also be adjusted from the computer to obtain the desired bed pressure drop and hence the expanded bed height. The interface between

the controller and driving motors of fuel and sorbent feeders and bed ash drain are provided with three speed transmitters. Cyclone ash and bed ash are collected in respective bins and their flow rates are followed by load cells placed under respective bins.

The volumetric flow rate of air is measured by a vortex flow meter and adjusted with an automatic butterfly valve driven by a computer controlled pneumatic actuator. In order to achieve conversion from volumetric to molar flow, a static pressure tap and a temperature sensor is placed downstream of the vortex flow meter. The flow rate of air is normally set to a value to achieve the desired superficial velocity in the combustor. In order to achieve almost neutral pressure on the bed surface, the flow rate of exhaust gases is adjusted with an automatic butterfly valve driven by a computer controlled pneumatic actuator.

In order to measure flow rates of cooling-water flowing through bed and cooler bundles, two orifices are located up streams of their lower and upper headers, respectively. The pressure drops across the orificemeters are measured by means of pressure transmitters. The signals from the transmitters are interpreted in the control system to yield mass flow rate of the cooling-water flowing through in-bed and cooler bundles. There exist two manual control valves installed on the downstream of upper and lower headers of bed and cooler bundles, respectively, to adjust the cooling-water flow in each bundle. The flow rates of cooling-water in bed and cooler bundles are normally set to a value which provide exit water temperature in the range 40-60 °C.

The on-line continuous gas analyzers with which the test rig is equipped are listed in Table 3.2. Analyzers except Bailey SMA 90 are used for measuring spatial variation of species O_2, CO, CO_2, SO_2 and NO/N_2O along the combustor at the positions given in Table 3.1 on dry basis. Bailey SMA 90 uses close-coupled sampling system which does not remove water vapor from the sample. The analyzer reports CO equivalent combustibles present in the flue gas. It is used for measuring temporal variation of O_2 and CO at the combustor exit.

Table 3.2: On-line gas analyzers.

Instrument	**Gas Species**
Bailey SMA 90	O_2, CO
Siemens Ultramat 6	SO_2
ABB advanced optima (Magnos 106)	O_2
ABB advanced optima (Uras 14)	CO, CO_2, NO, N_2O

Pressure sensors are used for measuring differential and gauge pressures at various positions on the test rig. Measured differential pressures are the pressure drops over orificemeters, bed and distributor plate pressure drop, and gauge pressures are the pressure at the bed surface and pressure of air feed at the downstream of the vortex flow meter. Also an orifice meter is placed before the ID fan ensuring that the flow rate of stack gas is determined.

Spatial and temporal variations of gas temperatures along the height of the combustor are measured by means of thermocouples of K type (Chromel-Alumel) with grounded junction to minimize their response time. The tips of the thermocouples are on the symmetry axis of the combustor. The axial positions of thermocouples are given in Table 3.3. The temperature of air feed at the downstream of vortex flow meter and temperatures of cooling water at the exits of bed and cooler bundles are measured by resistance thermocouples of type Pt-100. Further details of the test rig and operating procedures such as procedures before cold start-up, during runs, after shut down can be found elsewhere [40].

Table 3.3: Relative positions of thermocouples.

Thermocouple No	**Distance above the distributor plate,** *cm*
TC1	25
TC2	44
TC3	73
TC4	73
TC5	97
TC6	133
TC7	154
TC8	226
TC9	257
TC10	285
TC11	330
TC12	361
TC13	425
TC14	500

3.3 Experimental Conditions

3.3.1 Operating Conditions

Four experiments are carried out within the scope of this thesis study. In the first run (Run 1), only lignite is burned without limestone addition. In the following runs limestone addition is taken into consideration. In Run 5, lignite is co-fired with biomass with a share of 49 % on weight basis. Operating conditions of runs used in this study are tabulated in Table 3.4.

Table 3.4: Operating conditions of experiments.

Parameter	**Run 1**	**Run 2**	**Run 5**
Coal flow rate (kg/h)	76.5	68.7	30.2
Olive residue flow rate (kg/h)	0.0	0.0	28.8
Ca/S molar ratio	0.0	2.7	3.3
Air flow rate ($kmol/h$)	16.0	14.0	14.0
Superficial velocity (m/s)	2.2	1.9	1.9
Excess air (%)	19	15	27
Average bed temperature (°C)	894	848	852
Bed height (m)	1.00	1.10	1.10
Bed cooling water flow rate (kg/h)	3629	2842	3165
Freeboard cooling water flow rate (kg/h)	1792	2767	2691

3.3.2 Fuel and Sorbent Characteristics

Experiments were carried out with Çan lignite and olive residue. Biomass and crushed lignite were transported to the laboratory in bags. Lignite is sieved through 10 mm screen to remove possible uncrushed particles. The sieve analysis

of the lignite and biomass together with their calculated Rosin-Rammler function parameters can be found in Appendix A.

To understand the characteristics of fuels, its essential to make ultimate and proximate analyses of the samples. Samples are collected during the experiments by removing equal amount of substance in predetermined time intervals from the feeders hoopers under the respective fuel silos and subjected to sieve analyses. Then representative sample is divided and prepared for ultimate and proximate analysis. For that purpose samples are crushed under 200 μm. Wet samples are send to Normlab where proximate analyses are performed. Ultimate analysis of dried samples carried out in METU Central Laboratory. Details of the analyses can be found elsewhere [41, 42]. Proximate and ultimate analysis of the fuels together with their sieve analysis and calorific values are summarized in Tables 3.5 to 3.8. As can be seen from the tables lignite used in the experiments is characterized by its high VM/FC ratio ($\sim$1.2), high ash content ($\sim$ %26) and high total sulfur content ($\sim$ %3.5). On the other hand biomass almost contains no ash and sulfur and its VM/FC ratio ($\sim$5) is much higher than that of lignite.

Limestone utilized in the firing tests was supplied by Park Thermic, Electric Industry and Trade, Inc. and originates from Acıbaşı limestone quarry, 10 km away from the Çayırhan Thermal Power Plant. Limestone delivered to the laboratory had a particle size below 6 cm. It was subjected to size reduction by crushing it in a jaw-crusher and a hammer mill consecutively. Crushed limestone was sieved through a 1.18 mm sieve and top product was crushed again by hammer mill. Particles under the sieve were utilized in the experiments. The sieve analysis and fitted Rosin-Rammler parameters of limestone can be found in Appendix A.

Table 3.5: Characteristics of lignite used in Run 1.

Sieve Analysis		**Proximate Analysis (as received)**		**Ultimate Analysis (dry)**	
Size (*mm*)	**Weight** (%)	**Component**	**Weight** (%)	**Component**	**Weight** (%)
16.000 - 4.750	15.1	Moisture	16.3	C	44.7
4.750 - 3.350	16.9	Ash	28.8	H	3.9
3.350 - 2.000	13.6	VM	29.8	O	13.0
2.000 - 1.000	21.4	FC	25.1	N	1.0
1.000 - 0.500	10.8	LHV: 2943 (cal/g)		S_{comb}	3.0
0.500 - 0.355	5.9	d_{32}: 0.430 *mm*		S_{tot}	4.2
0.355 - 0.000	16.3	ρ_p: 1.506 g/cm^3		Ash	34.4

Table 3.6: Characteristics of lignite used in Run 2.

Sieve Analysis		**Proximate Analysis (as received)**		**Ultimate Analysis (dry)**	
Size (*mm*)	**Weight** (%)	**Component**	**Weight** (%)	**Component**	**Weight** (%)
16.000 - 4.750	30.1	Moisture	16.5	C	44.9
4.750 - 3.350	23.4	Ash	26.7	H	4.0
3.350 - 2.000	13.3	VM	31.1	O	15.5
2.000 - 1.000	14.2	FC	25.7	N	1.1
1.000 - 0.500	5.5	LHV: 3165 (cal/g)		S_{comb}	2.5
0.500 - 0.355	2.8	d_{32}: 0.581 *mm*		S_{tot}	4.0
0.355 - 0.000	10.9	ρ_p: 1.506 g/cm^3		Ash	32.0

Table 3.7: Characteristics of lignite used in Run 5.

Sieve Analysis		**Proximate Analysis (as received)**		**Ultimate Analysis (dry)**	
Size (*mm*)	**Weight** (%)	**Component**	**Weight** (%)	**Component**	**Weight** (%)
16.000 - 4.750	23.2	Moisture	16.8	C	44.8
4.750 - 3.350	26.1	Ash	23.9	H	4.0
3.350 - 2.000	14.1	VM	32.0	O	17.9
2.000 - 1.000	15.2	FC	27.3	N	1.2
1.000 - 0.500	6.1	LHV: 3343 (cal/g)		S_{comb}	3.4
0.500 - 0.355	3.2	d_{32}: 0.585 *mm*		S_{tot}	3.6
0.355 - 0.000	12.1	ρ_p: 1.506 g/cm^3		Ash	28.7

Table 3.8: Characteristics of olive residue used in Run 5.

Sieve Analysis		**Proximate Analysis (as received)**		**Ultimate Analysis (dry)**	
Size (*mm*)	**Weight** (%)	**Component**	**Weight** (%)	**Component**	**Weight** (%)
6.300 - 3.350	12.0	Moisture	6.1	C	50.2
3.350 - 2.000	21.5	Ash	4.2	H	6.4
2.000 - 1.000	20.8	VM	75.7	O	37.1
1.000 - 0.500	13.7	FC	14.0	N	1.7
0.500 - 0.355	9.4	LHV: 4312 (cal/g)		S_{comb}	0.1
0.355 - 0.180	9.3	d_{32}: 0.360 *mm*		S_{tot}	0.1
0.180 - 0.000	13.3	ρ_p: 1.060 g/cm^3		Ash	4.5

CHAPTER 4

RESULTS AND DISCUSSION

The accuracy of the present system model is tested by predicting the behavior of the 0.3 MW ABFBC test rig for operating conditions shown in Table 3.4 and comparing the predictions with measurements. Axial temperature profiles, concentration profiles of O_2, CO, CO_2, SO_2 and NO throughout the combustor, gaseous emissions were used as measures of performance to test the validity of the model.

The input data required by the model includes the following:

- Configuration and dimensions of the test rig and its internals.
- Air and fuel flow rates.
- Coal, biomass and limestone analyses.
- All solid and gas properties.
- Coal and biomass partitioning into char and volatile nitrogen
- Size distribution function of feed solids deduced from sieve analysis.
- Inlet temperatures of air, cooling water, and feed solids.

4.1 Volatiles Release in Bed

To better understand devolatilization characteristics of samples TGA tests are performed. As can be observed from Figure 4.1, gasification of olive residue takes place in two consecutive steps. The first step is drying, which occurs about

100-150 °C. During this step bound water is removed from the sample. In the next step, devolatilization takes place. As can be seen from the figures, differential weight loss curve for low heating rate (40 K/min) involves two steps of devolatilization. These two steps are due to degradation of different compounds in the fuel sample as also reported in literature [43]. However, at higher heating rate (100 K/min), these two steps can not be differentiated due to much faster pyrolysis.

For coal, drying occurs at similar temperatures to olive residue. However, similarity for releases of volatiles between coal and olive residue can not be observed. As can be seen form Figure 4.2, coal releases its volatiles at relatively higher temperatures ($\sim$ 450-500 °C.) Moreover, duration of volatile release by coal takes longer compared olive residue. The reason for this might be the composition of coal.

Volatile release model described in Section 2.2.2 was applied to the test rig for both coal and biomass. The quantity of volatiles released in the bed was determined by combining the results of particle model with time resolved devolatilization profile. The time-resolved devolatilization profile of coal and biomass of average diameter were computed from the simultaneous solution of Equations (2.9) and (2.10). The kinetic parameters appearing in Equation (2.9) were obtained by performing thermogravimetric analysis (TGA) for coal and biomass and fitting the weight loss data gathered during TGA analyses for these parameters. The details of TGA runs and fitting process are given in Appendix B. The fraction of volatiles released in bed section is found 0.78 for coal and 1.00 for olive residue.

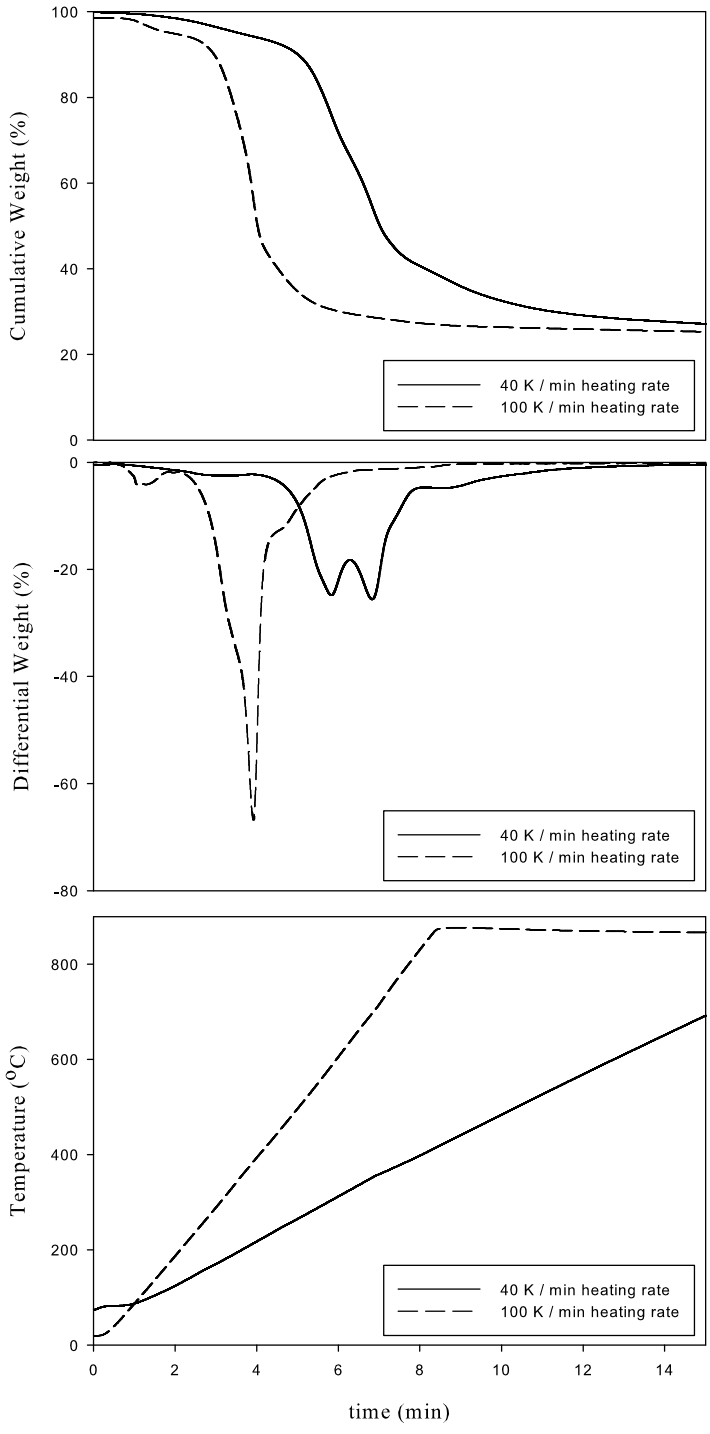

Figure 4.1: TGA analysis of olive residue.

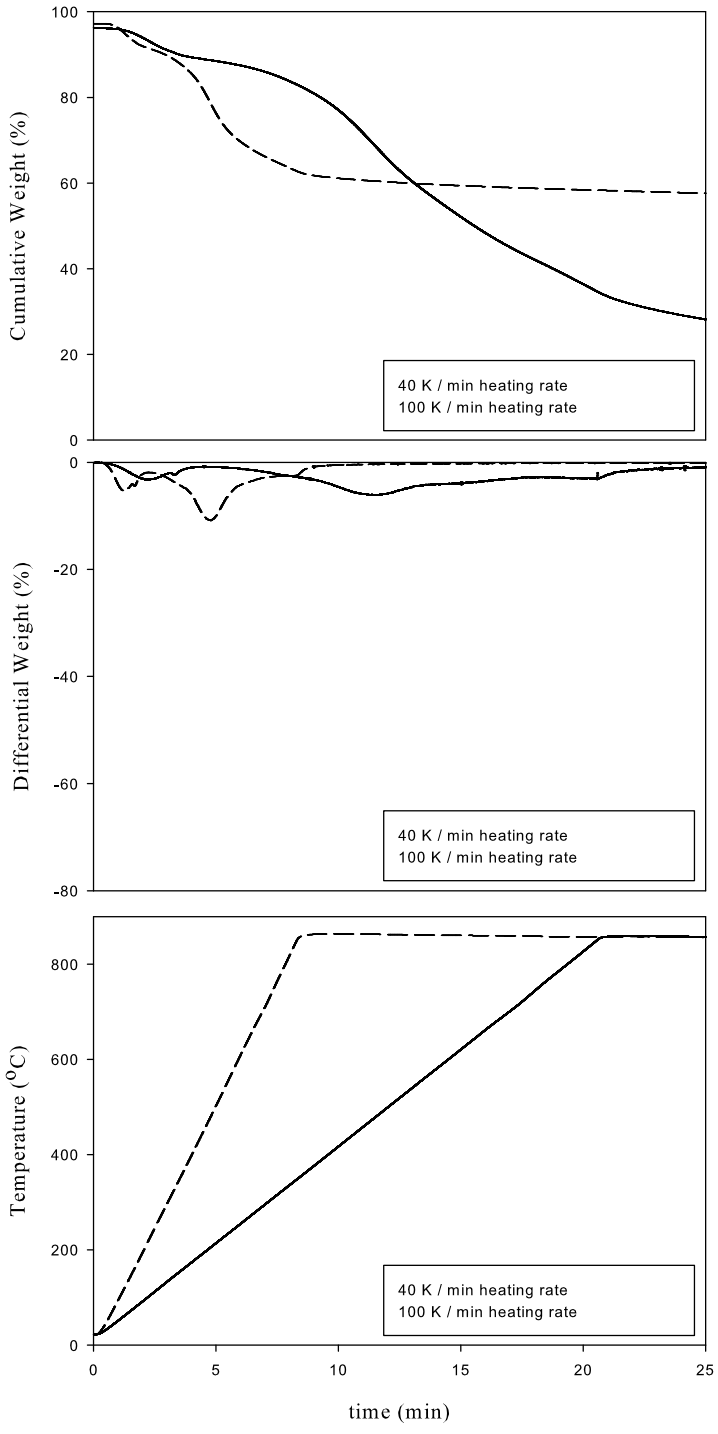

Figure 4.2: TGA analysis of coal.

4.2 Temperature Profiles

Figures 4.3-4.5 illustrate comparison between the predicted and measured temperatures along the combustor for the experiments under consideration. Predicted profiles and the measured values are found to be in reasonable agreement except for Run 5. In Run 5 model predictions resulted in higher overall temperatures compared to experimental measurements. However the trend of temperature profile is similar to experimental data. Discrepancies between measured and predicted temperature profile of Run 5 may be considered to be due to rapid combustion of high amount of volatile matter in bed section. The fall in the gas temperature toward the exit is due to the presence of cooler in the final module.

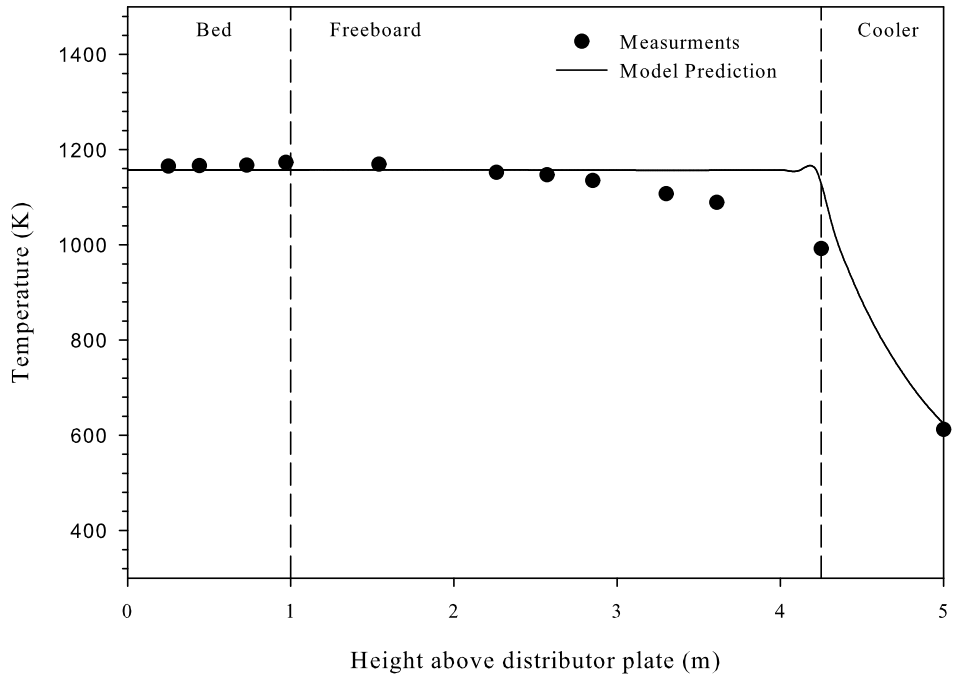

Figure 4.3: Measured and predicted temperature profiles for Run 1.

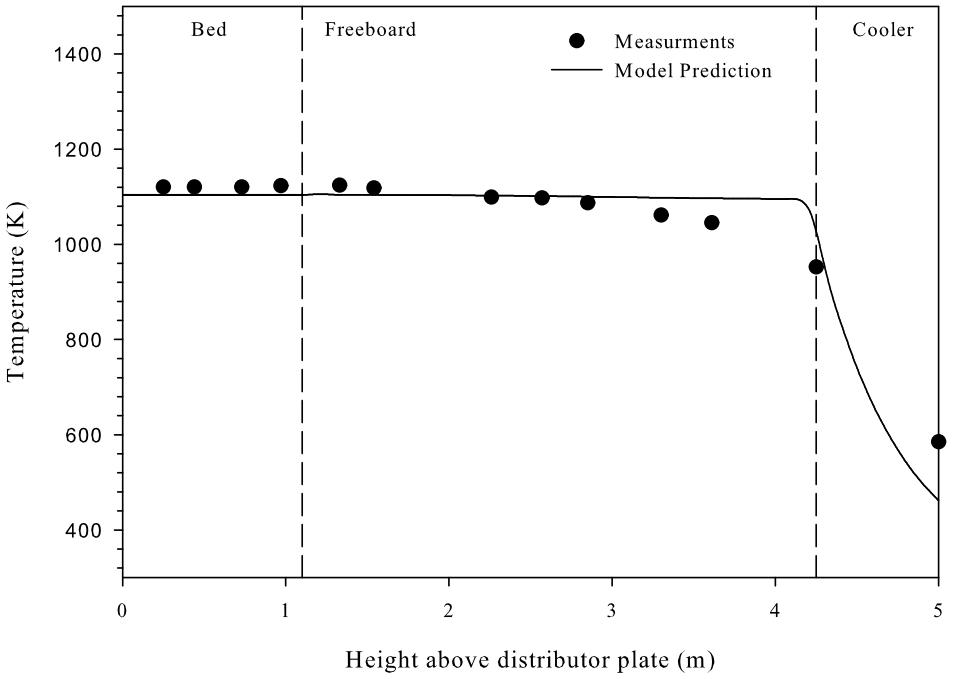

Figure 4.4: Measured and predicted temperature profiles for Run 2.

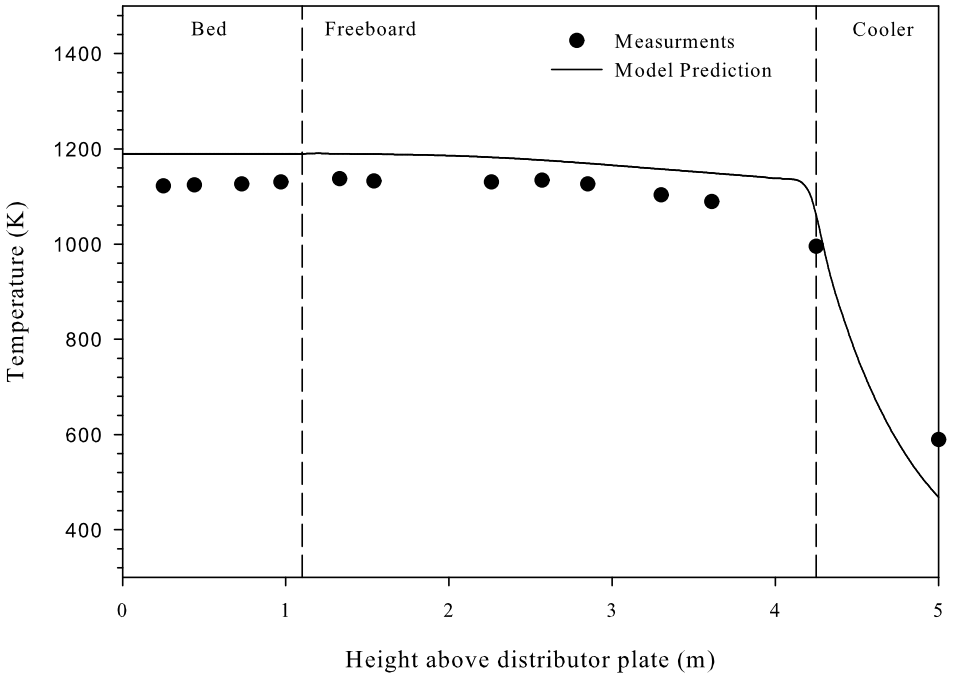

Figure 4.5: Measured and predicted temperature profiles for Run 5.

4.3 O_2, CO_2 and CO Concentration Profiles

Figures 4.6-4.8 compare the predicted and measured concentrations of O_2, CO_2 and CO along the combustor for Run 1, Run 2 and Run 5, respectively. As can be seen from the figures, measured O_2 concentrations decrease until the bed surface whereas the measured CO_2 concentrations display an opposite trend in the same region, as expected. As for the freeboard section, the decrease in O_2 and increase in CO_2 concentrations keep on but with a lower slope. CO measurements, on the other hand, show maxima in the bed and decrease gradually along the freeboard with a lower slope. That is mainly due to presence of CO in oxygen lean emulsion phase. Details of pre-exponential factor for CO combustion rate on CO concentration can be found in Appendix C.

The effect of co-firing with biomass on the concentration profiles can best be illustrated by comparing oxygen consumption in freeboard in Runs 2 and 5. Percentage oxygen consumptions in freeboard are found to be around 10 and 8, during combustion of lignite with and without biomass, respectively. This is considered to be due to introduction of higher volatile matter with biomass leading to passage and combustion of volatile matter in freeboard. Predicted percentage oxygen consumption in freeboard with and without biomass combustion are found to be 7 and 9, respectively. These values agree favorably well with the measurements.

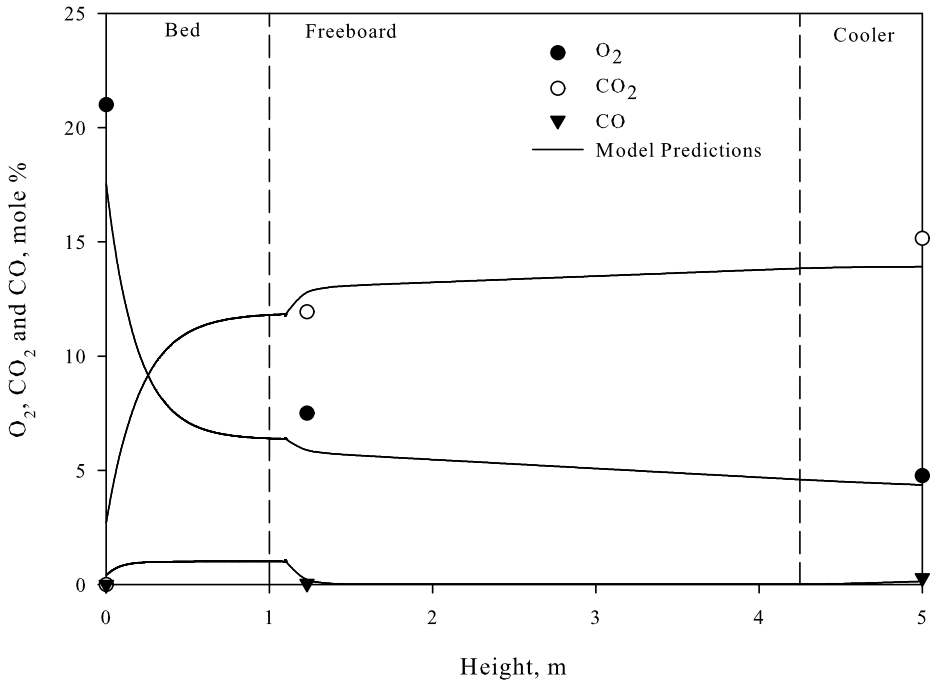

Figure 4.6: Measured and predicted O_2, CO_2 and CO concentrations for Run 1.

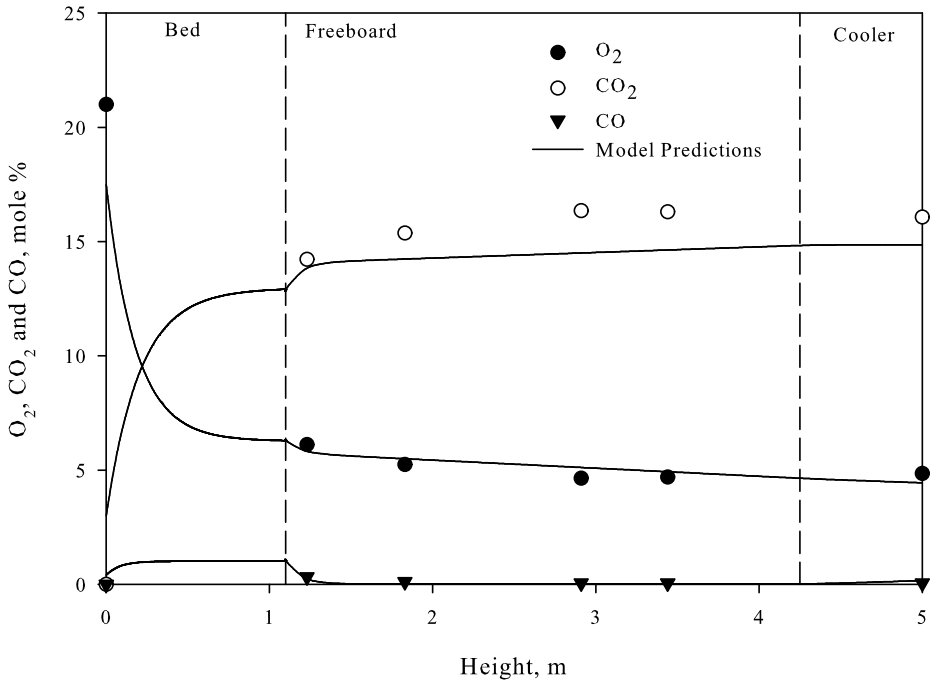

Figure 4.7: Measured and predicted O_2, CO_2 and CO concentrations for Run 2.

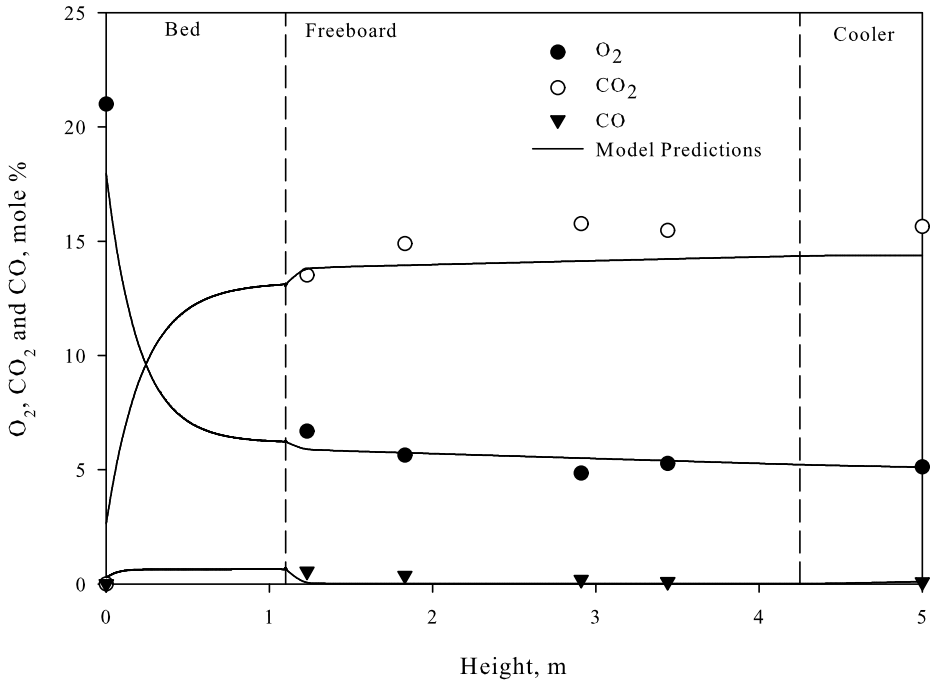

Figure 4.8: Measured and predicted O_2, CO_2 and CO concentrations for Run 5.

4.4 SO_2 and NO Concentration Profiles

Figures 4.9-4.11 compare the predicted and measured concentrations of SO_2 and NO along the combustor for Run 1, Run 2 and Run 5, respectively. As can be observed from the figures, SO_2 concentration in Run 1 is highest decreasing with addition of limestone in Run 2. In Run 5 with 49 % biomass share SO_2 concentration decreased further due to low sulfur content of olive residue. Inspection of the figures reveal that SO_2 concentration continues to increase from bed exit to the combustor exit. This may be owing to the absence of sulfur capture as well as to progressive release of volatiles.

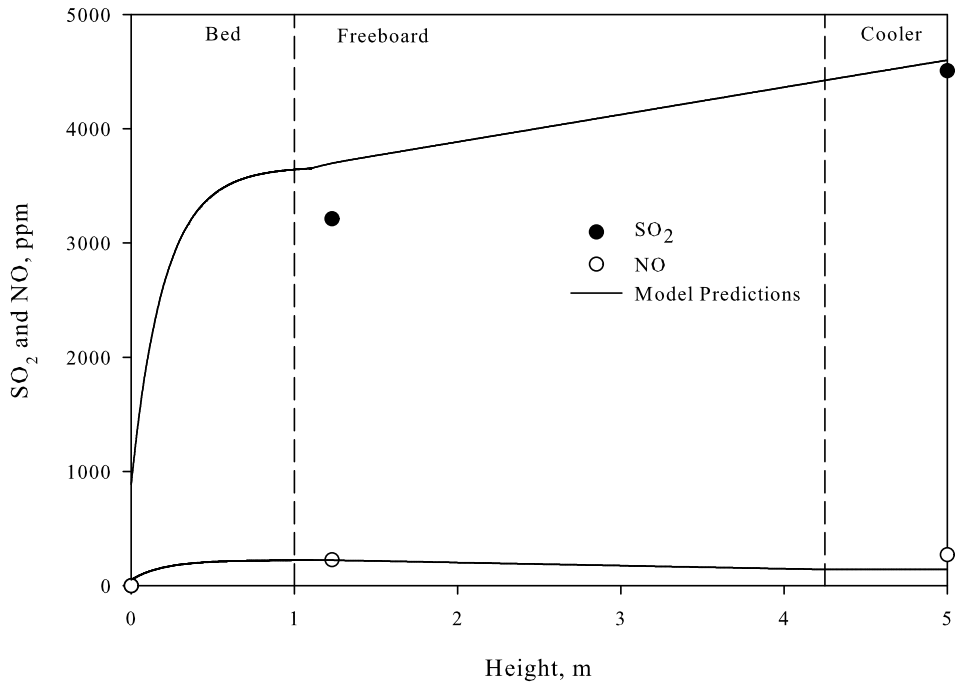

Figure 4.9: Measured and predicted SO_2 and NO concentrations for Run 1.

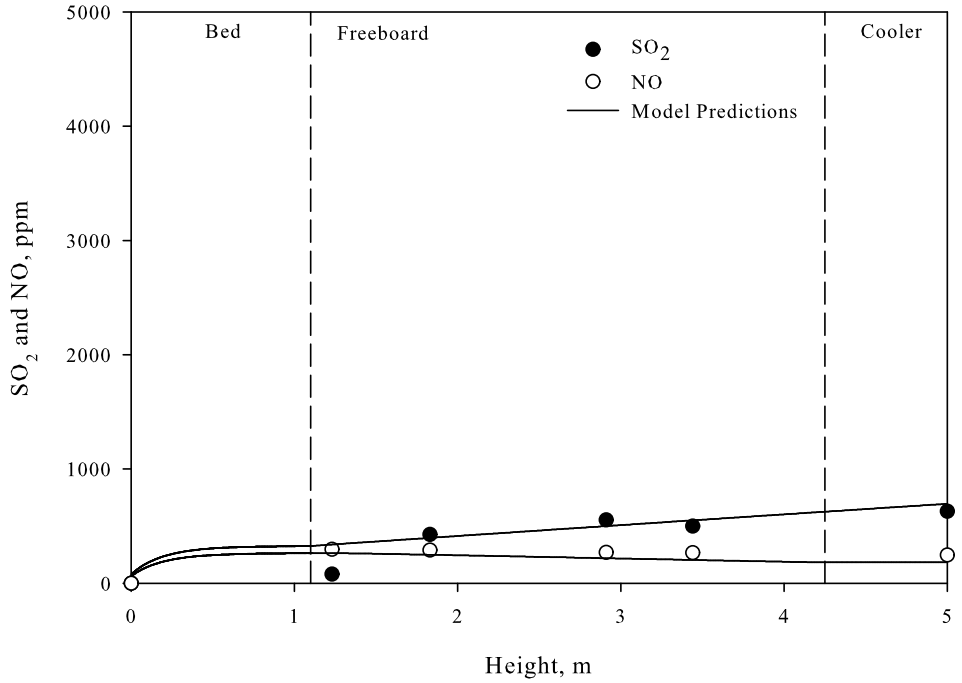

Figure 4.10: Measured and predicted SO_2 and NO concentrations for Run 2.

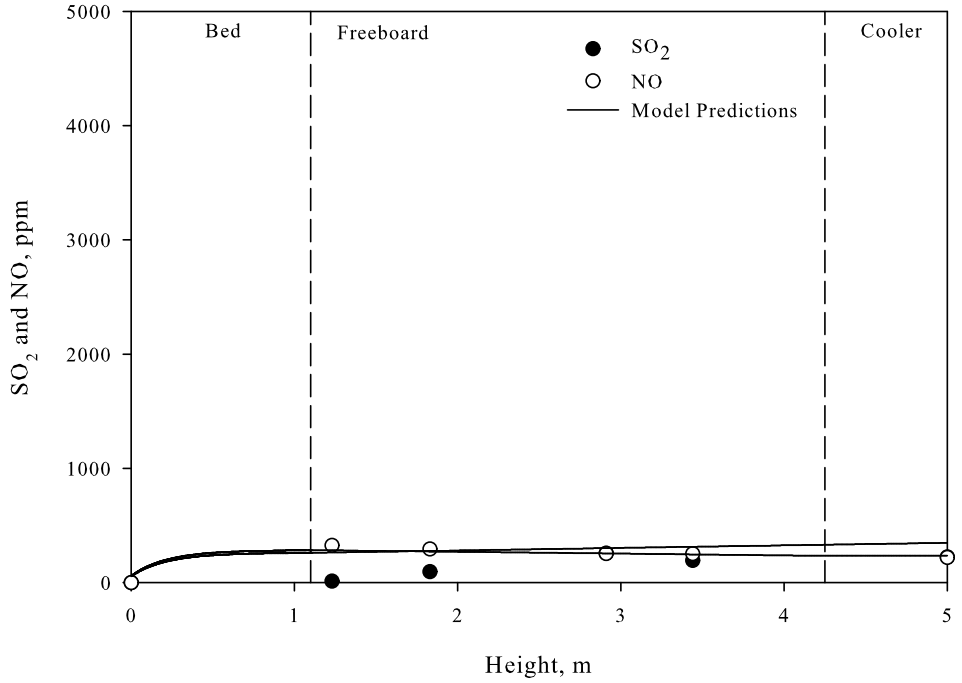

Figure 4.11: Measured and predicted SO_2 and NO concentrations for Run 5.

CHAPTER 5

CONCLUSIONS

Co-combustion of lignite and biomass is investigated by extending a previously developed system model for co-firing lignite with biomass. The system model accounts for hydrodynamics, volatiles release and combustion, char combustion, particle size distribution, entrainment, elutriation, sulfur retention, and NO formation and reduction, and is based on conservation equations for energy and chemical species. The predictive performance of the model was tested by comparing model predictions with experimental measurements obtained from combustion tests carried out by co-firing lignite with biomass in a 0.3 MWt atmospheric bubbling fluidized bed combustor.

On the basis of the experimental observations and comparisons of the model predictions with measurements, the following conclusions have been reached:

- O_2, CO, CO_2, SO_2 and NO concentration profiles and temperature profile predictions of the model are generally in good agreement with the experimental data.
- SO_2 emissions decrease considerably when lignite is co-fired with biomass.
- NO emissions are not significantly affected by addition of biomass.

5.1 Suggestion for Future Work

Based on the experience gained in the present study, use of different volatile release submodels reported in the literature in conjunction with the system model proposed in this study and validation against experimental data obtained in this study is recommended.

REFERENCES

[1] Armesto L., Veijonen K., and Bahillo A., "Co-combustion of coal and biomass wastes in fluidized bed," in *International Conference on Fluidized Bed Combustion*. ASME, 2001.

[2] Gayan P., Adanez J., de Diego L. F., Garcia-Labiano F., Cabanillas A., Bahillo A., Aho M., and Veijonen K., "Circulating fluidized bed co-combustion of coal and biomass," *Fuel*, vol. 83, no. 3, pp. 277–286, 2004.

[3] Hupa M., "Interaction of fuels in co-firing in FBC," *Fuel*, vol. 84, no. 10, pp. 1312–1319, 2005.

[4] Sami M., Annamalai K., and Wooldridge M., "Co-firing of coal and biomass fuel blends," *Progress In Energy And Combustion S*, vol. 27, no. 2, pp. 171–214, 2001.

[5] Scala F. and R. Chirone, "Fluidized bed combustion of alternative solid fuels," *Experimental Thermal And Fluid Scie*, vol. 28, no. 7, pp. 691–699, 2004.

[6] Okasha F., "Modeling of straw-bitumen pellets in fluidized bed," *Fuel Processing Technology*, vol. 88, pp. 281–293, 2007.

[7] Adanez J., Gayan P., de Diego L. F., Garcia-Labiano F., and Abad A., "Combustion of wood chips in a CFBC. modeling and validation," *Industrial & Engineering Chemistry*, vol. 42, no. 5, pp. 987–999, 2003.

[8] Selçuk N. and Sivrioğlu Ü., "Mathematical modeling of coal-fired fluidized beds," *Journal of Thermal Sciences and Technology (in Turkish)*, vol. 3, no. 1, pp. 31–38, 1980.

[9] Afacan O., Göğebakan Y., and Selçuk N., "Modeling of NO_X emissions from fluidized bed combustion of high volatile lignites," *Combustion Science and Technology*, vol. 179, no. 1-2, pp. 227–247, 2007.

[10] Selçuk N., Değirmenci E., and Göğebakan Y., "Modeling of a bubbling AFBC with volatiles release," *Journal Of Energy Resources Technology*, vol. 125, no. 1, pp. 72–81, 2003.

[11] Afacan M. O., "Mathematical modeling of NO_X in bubbling fluidized bed combustors," M.S. thesis, Department of chemical engineering, METU, 2005.

[12] Adanez J., de Diego L. F., Garcia-Labiano F., Abad A., and Abanades J. C., "Determination of biomass char combustion reactivities for fbc applications by a combined method," *Industrial & Engineering Chemistry*, vol. 40, no. 20, pp. 4317–4323, 2001.

[13] Field M.A., Gill D.W., Morgan B.B., and Hawkesley P.G.W., *Combustion of pulverized coal*, British Coal Utilization Research Association, 1967.

[14] Hottel H.C., Williams G.C., Nerheim N.M., and Schneider G.R., "Kinetic studies on stirred reactors, combustion of carbon monoxide and propane," in *Proceedings of the 10th Int. Symp. on combustion*. ASME, 1965, vol. 1, pp. 975–986.

[15] Altındağ H., Göğebakan Y., and Selçuk N., "Sulfur capture for fluidized bed combustion of high sulfur content lignites," *Applied Energy*, vol. 79, no. 4, pp. 403–424, 2004.

[16] Duo W., Dam-Johansen K., and Ostergaard K., "Kinetics of the gas-phase reaction between nitric-oxide, ammonia and oxygen," *Canadian Journal of Chemical Engineering*, vol. 70, no. 5, pp. 1014–1020, 1992.

[17] Johnsson J.E. and Dam-Johansen K., "Formation and reduction of NO_X in a fluidized bed combustor," in *11th International Conference on Fluidized Bed Combustion*. ASME, 1991, pp. 1389–1396.

[18] Jung K. and La Nauze R. D., ," in *Proceedings of the the fourth International Conference On Fluidization*. Engineering Foundation.

[19] Incropera F.P. and De Witt D.P., *Fundamentals of Heat and Mass Transfer*, John Wiley and Sons, 4st edition, 2001.

[20] Choi J.H., Chang I.Y., Shun D.W., Yi C.K., Son J.E., and Kim S.D., "Correlation on the particle entrainment rate in gas fluidized beds," *Ind. Eng. Chem. Res.*, vol. 38, pp. 2491–2496, 1999.

[21] Kunii D. and Levenspiel O., *Fluidization Engineering*, Butterworth Heinemann, 2nd edition, 1991.

[22] Gogolek P.E.G. and Becker H.A., "Calculation of the expansion of a bubbling

fluidized bed of coarse particles," *Powder Technology*, vol. 71, pp. 107–110, 1992.

[23] Ergun S., "Fluid flow through packed columns," *Chemical Engineering Progress*, vol. 48, no. 2, pp. 89–94, February 1952.

[24] Mori S. and Wen C. Y., "Estimation of bubble diameter in gaseous fluidized beds," *AIChE Jounal*, vol. 21, no. 1, pp. 109–116, January 1975.

[25] Davidson J.F. and Harrison D., *Fluidized Particles*, Cambridge University Press, 1963.

[26] Danloye A.O.O. and Botterill J.S.M, "Bed to surface heat-transfer in a fluidized bed of large particles," *Powder Technolgy*, vol. 19, no. 2, pp. 197–203, 1978.

[27] Sleicher C. A. and Rouse M. W., "A convenient correlation for heat transfer to constant and variable property fluids in turbulent pipe flow," *Internationa Journal of Heat and Mass Transfer*, vol. 18, pp. 677–683, 1975.

[28] Grace J.R. and Clift R., "On the two-phase theory of fluidization," *Chemical Engineering Science*, vol. 29, pp. 327–334, 1974.

[29] Grace J.R. and Harrison D., "The behaviour of freely bubbling fluidized beds," *Chemical Engineering Science*, vol. 24, pp. 497–508, 1969.

[30] Stubington J. F., Chan S. W., and Clough S. J, "A model for volatiles release into a bubbling fluidized bed combustor," *AIChE Journal*, vol. 36, no. 1, pp. 75–85, 1990.

[31] Fiorentino M. and Marzocchella A.and Salatino P., "Segregation of fuel particles and volatile matter during devolatilization in a fluidized bed reactor.2. experimental," *Chemical Engineering Science*, vol. 52, no. 12, pp. 1909–1922, 1997.

[32] Anthony D. B. and J. B. Howard, "Coal devolatilization and hydrogasification," *Aiche Journal*, vol. 22, no. 4, pp. 625–656, 1976.

[33] Göğebakan Y., "Char attrition in fluidized bed combustors," M.S. thesis, Department of chemical engineering, METU, 2000.

[34] Altındağ H., "Mathematical modeling of sulfur retention in fluidized bed combustors," M.S. thesis, Department of chemical engineering, METU, 2003.

[35] Hazlett J.D. and Bergougnou M.A., "Influence of bubble size distribution at the bed surface on entrainment profile," *Powder Technology*, vol. 70, pp. 99–107, 1992.

[36] Hannes J., *Mathematical Modeling of Circulating Fluidized Bed Combustion*, Ph.D. thesis, RWTH, Aachen, Germany, 1996.

[37] Radhakrishnan K. and Hindmarsh A. C., "Description and use of LSODE, the livermore solver for ordinary differential equations," *Lawrance Livermore National Laboratory Report No: UCRL-ID-113855*, 1993.

[38] Değirmenci E., *Dynamic Simulation of Fluidized Bed Combustors*, Ph.D. thesis, Department of Chemical Engineering ,METU, Ankara, Turkey, 2000.

[39] Anthony E.J., Couturier M.F., and Briggs D.W., "Gas sampling at the point tupper afbc facility," *CANMET, Energy, Mines and Resources, Division Report 86-70*, 1986.

[40] Harmandar H., "Effect of recycling on the performance of bubbling fluidized bed combustors," M.S. thesis, Department of chemical engineering, METU, 2003.

[41] Last access: 29.06.2007, "http://www.normlab.com/hizmetlerimiz.htm," *Normlab İvedik Org. San. Sit. 22. Cad. 681 Sok. No.17 Ostim-Ankara*.

[42] Last access: 29.06.2007, "http://www.centrallab.metu.edu.tr," *ODTÜ Merkezi Laboratuvar AR-Ge Eğitim ve Ölçme Merkezi 06531 ANKARA*.

[43] Jauhiainen J., Conesa J. A., Font R., and Gullón I. M., "Kinetics of the pyrolysis and combustion of olive solid waste," *Journal of Analytical and Applied Pyrolysis*, vol. 72, pp. 9–15, 2004.

APPENDIX A

PARTICLE SIZE DISTRIBUTION

A.1 Sieve Analysis

Table A.1: Sieve analysis of lignite

Size (*mm*)	**Weight** (%)		
	Run 1	**Run 2**	**Run 5**
16.000 - 12.700	1.078	2.033	0.458
12.700 - 8.000	3.042	8.434	4.450
8.000 - 6.300	4.896	9.236	7.982
6.300 - 4.750	6.103	10.413	10.380
4.750 - 3.350	16.859	23.378	26.056
3.350 - 2.000	13.565	13.265	14.099
2.000 - 1.000	21.478	14.160	15.252
1.000 - 0.500	10.851	5.553	6.142
0.500 - 0.355	5.823	2.687	3.167
0.355 - 0.180	5.553	2.555	3.298
0.180 - 0.106	4.094	2.681	3.950
0.106 - 0.000	6.659	5.606	4.766

Table A.2: Sieve analysis of olive residue

Size (*mm*)	**Weight** (%)
6.300 - 4.750	0.128
4.750 - 3.350	11.966
3.350 - 2.000	21.510
2.000 - 1.000	20.840
1.000 - 0.500	13.599
0.500 - 0.355	9.314
0.355 - 0.180	9.327
0.180 - 0.106	6.177
0.106 - 0.000	7.139

Table A.3: Sieve analysis of limestone

Size (*mm*)	**Weight** (%)
1.180 - 1.000	14.795
1.000 - 0.850	5.286
0.850 - 0.710	6.257
0.710 - 0.600	10.657
0.600 - 0.500	3.837
0.500 - 0.425	9.738
0.425 - 0.355	6.135
0.355 - 0.180	15.060
0.180 - 0.106	10.487
0.106 - 0.000	17.748

A.2 Rosin-Rammler Size Distribution Functions

The size distribution of lignite, biomass and limestone were determined by sieve analysis and were expressed by the following Rosin-Rammler size distribution function in the system model:

$$P_0(d_p) = exp\left(-b \cdot d_p^n\right) \tag{A.1}$$

Parameters b and n in (A.1) were calculated by using Sigma Plot 10.0. Calculated values of the coefficients can be found in Table A.4.

Table A.4: Rosin-Rammler function fitting results for solid feed streams

	n	b	**Standart Error**	**Correlation Coefficent**
Coal Run 1	0.90	3.41	0.02	1.00
Coal Run 2	1.09	2.55	0.04	0.99
Coal Run 5	1.12	3.06	0.04	0.99
Limestone	1.06	20.75	0.02	0.99
Olive Residue	0.95	5.74	0.03	0.99

In Figure A.1 to Figure A.5 fitted Rosin-Rammler forms of lignite, biomass and limestone are present. As it can be observed from figures, Rosin-Rammler function represents the size distributions accurately.

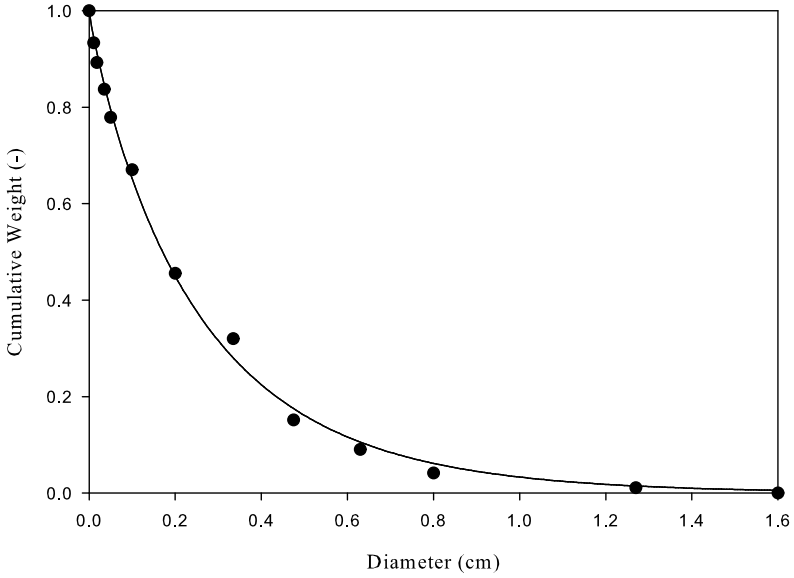

Figure A.1: Fitted Rosin-Rammler form of lignite (Run 1)

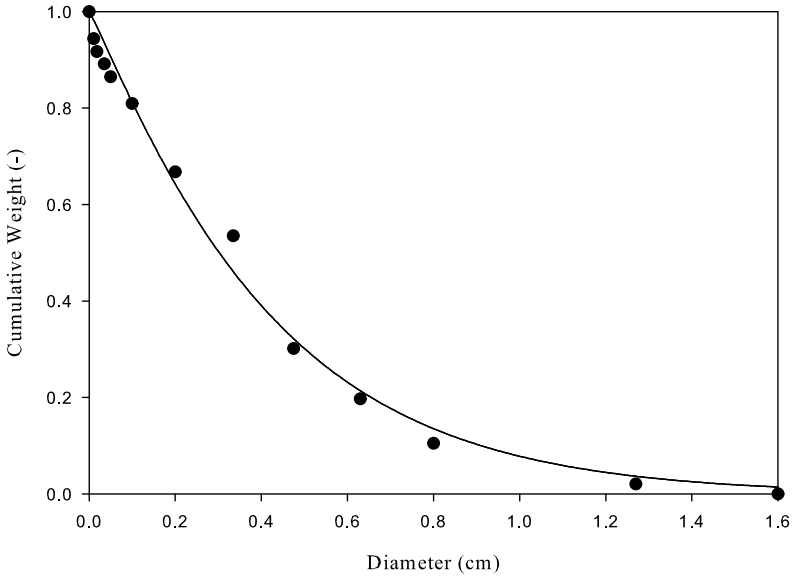

Figure A.2: Fitted Rosin-Rammler form of lignite (Run 2)

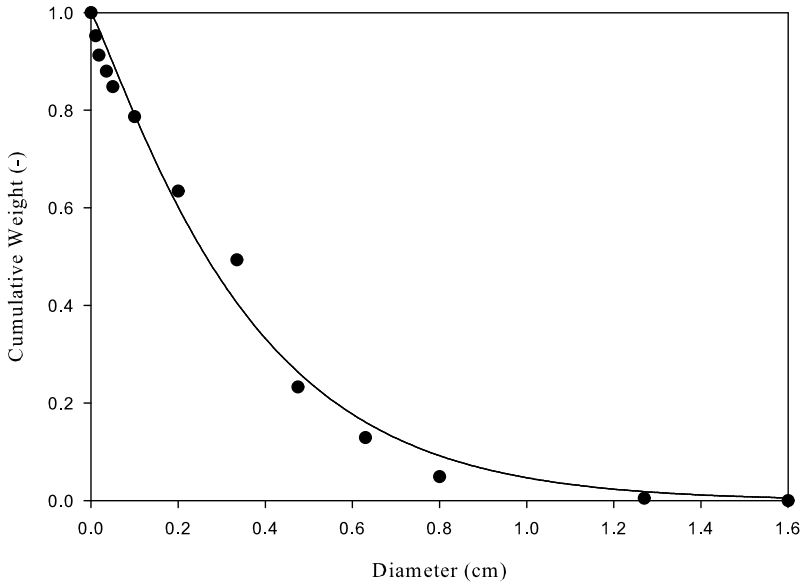

Figure A.3: Fitted Rosin-Rammler form of lignite (Run 5)

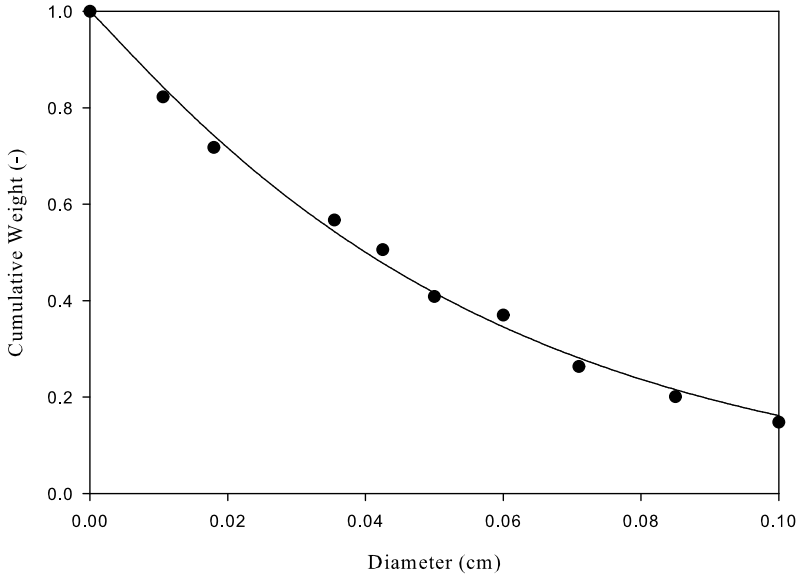

Figure A.4: Fitted Rosin-Rammler form of limestone

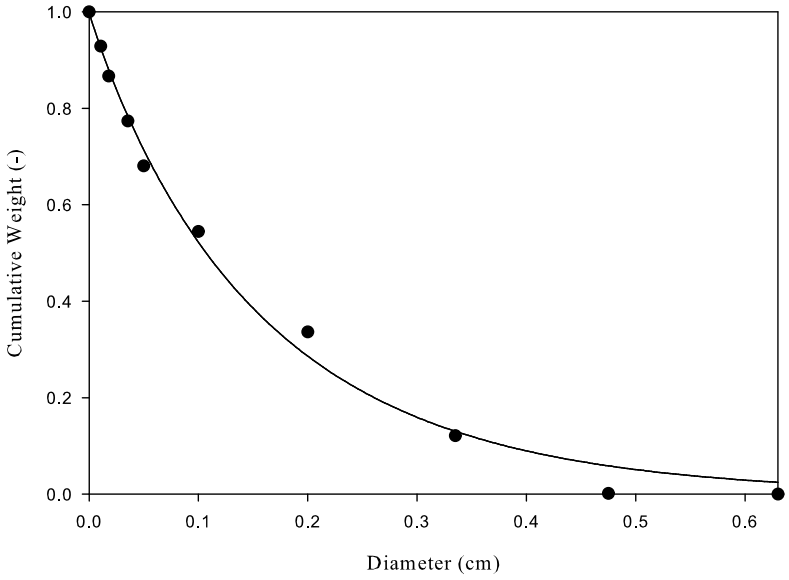

Figure A.5: Fitted Rosin-Rammler form of olive residue

APPENDIX B

Devolatilization Kinetics

The parallel independent reaction model of Anthony [32] was used to describe the devolatilization kinetics of fuels used in the experiment. The governing equations of the model are given in Section 2.2.2. Model equations contain four parameters to be estimated from experimental data: v_∞, k_0, E_0 and σ, which represent ultimate yield of volatiles, pre-exponential factor, mean activation energy and its standard deviation, respectively.

Experimental data on devolatilization kinetics was obtained from thermogravimetric analysis (TGA). To prepare samples for the test, representative samples are crushed under 250 μm and transported in closed bags to the laboratory. In TGA tests, samples are heated from ambient temperature to 850°C at two different heating rates (40 °C/min and 100 °C/min) in N_2 atmosphere and kept isothermal for one hour to reach constant weight.

The time versus weight loss data gained during TGA runs were used to obtain parameters v_∞, k_0, E_0 and σ. The ultimate yield of volatiles, v_∞, is determined from TGA data by converting ultimate volatile loss to dry basis, for both heating rates. As for the model parameter, k_0, a constant value of $1.3 \cdot 10^{13}$, suggested in [38], was used. The other two parameters E_0 and σ were determined by applying a non-linear fitting process to TGA data on weight loss versus time data for both heating rates.

Since powdered samples were used in TGA runs, in the fitting process the particles were assumed to be isothermal. Therefore, in this stage, Equation (2.8) rather than Equation (2.9) was used to describe the devolatilization of coal and biomass.

During the fitting process the following procedure suggested in [38] was employed for lignite and biomass:

1. Fit E_0 and σ to experimental data for both temperature ramps.
2. Average E_0's calculated in step 1 and fit experimental data for σ for both ramps.
3. Average σ's in step 2.

Average E_0 and σ values calculated in step 2 and 3 were accepted as kinetic parameters for each fuel. Calculated values of these parameters are presented in Table B.1.

Table B.1: Devolatilization kinetic parameters for lignite and olive residue.

	Lignite	**Olive residue**
E_0, $cal/mole$	61933	39272
σ,$cal/mole$	18481	16890

Figures B.1 and B.2 compare calculated and experimental weight losses for temperature ramps of 40 °C/min and 100 °C/min. As can be seen from figures, results obtained by using kinetic parameters listed in Table B.1 show good agreement with experimental data.

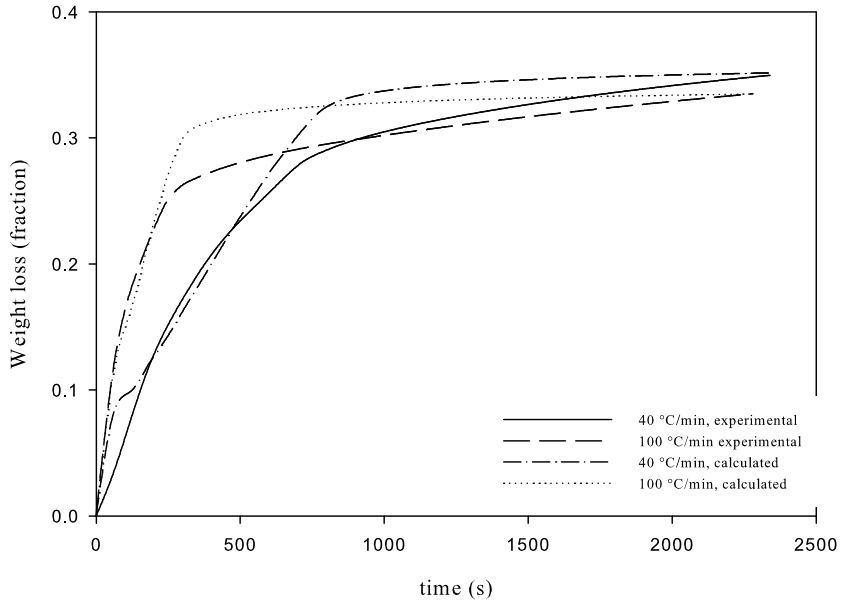

Figure B.1: Comparison of calculated and experimental weight losses for lignite.

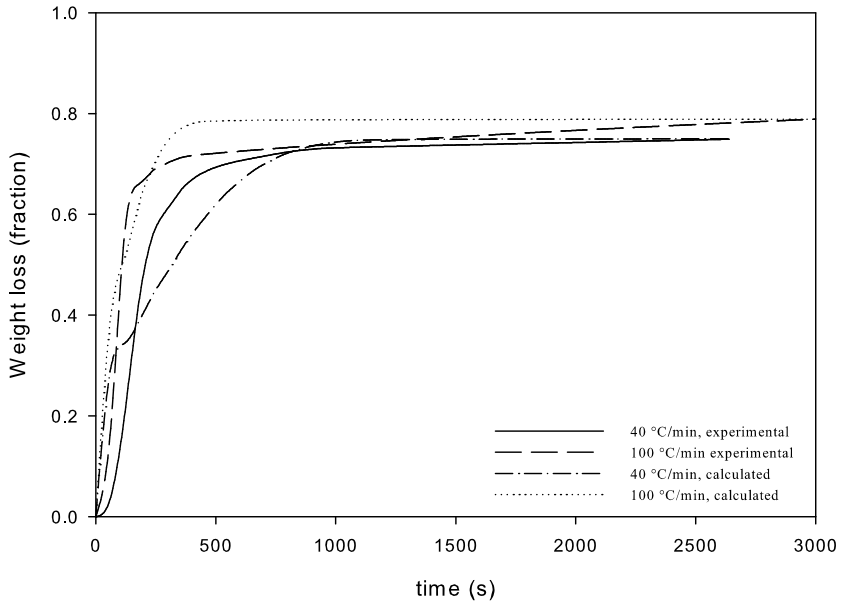

Figure B.2: Comparison of calculated and experimental weight losses for olive residue.

APPENDIX C

Effect of CO Combustion Rate

In the system model volatile carbon is assumed to be instantaneously oxidized to CO. Moreover, the product of char combustion is also CO. The pre-exponential factor for CO has been modified previously to handle fluidized bed combustion conditions [38]. Effect of the scaling on pre-exponential factor on CO concentration is presented in Figures C.3 to C.1. As can be observed from the figures, decreasing the pre-exponential factor increases CO concentration in bed section, as expected. The rapid consumption of CO in freeboard is mainly due to rapid mixing of emulsion phase and oxygen rich bubble phase. Despite scaling CO combustion rate by a factor of 0.1 resulted in relatively poor agreement with experimental measurements for Run 1 and Run 2, in-bed measurements of CO concentration in previous studies [40] on the same combustion chamber showed that concentration of CO in bed section is usually around 1%. Because of this reaseon and good agreement between experimantal measurments and model predictions in Run 5, the pre-exponential factor for CO combustion rate in overall system model is scaled by a factor of 0.1.

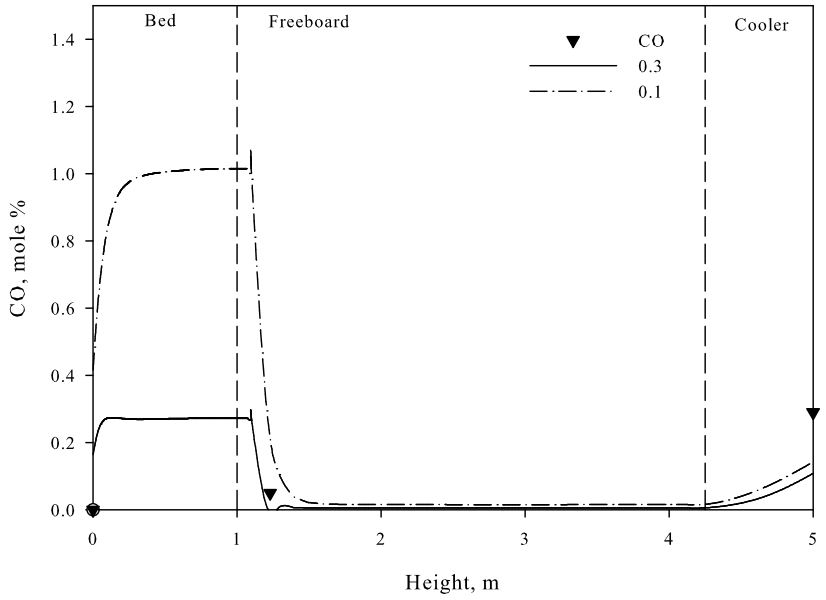

Figure C.1: Effect of scaling the pre-exponential factor on *CO* concentration in Run 1.

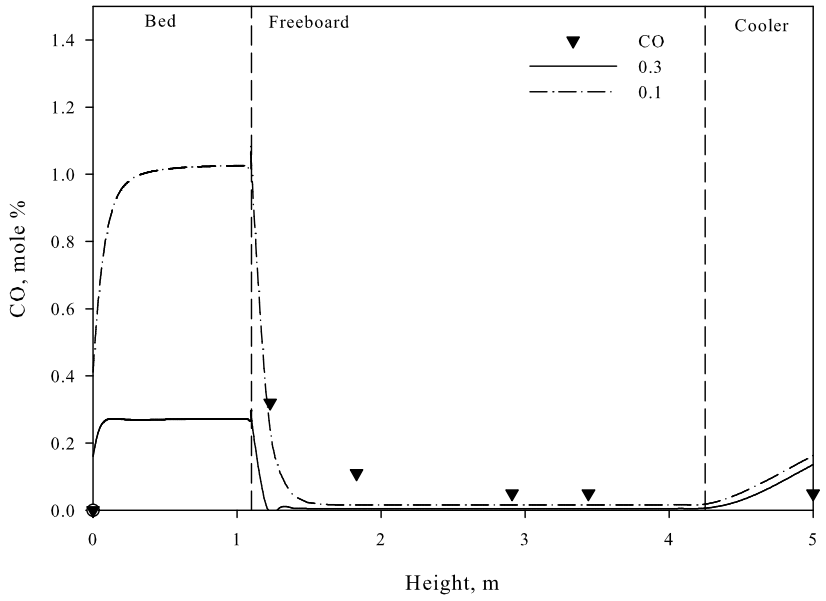

Figure C.2: Effect of scaling the pre-exponential factor on *CO* concentration in Run 2.

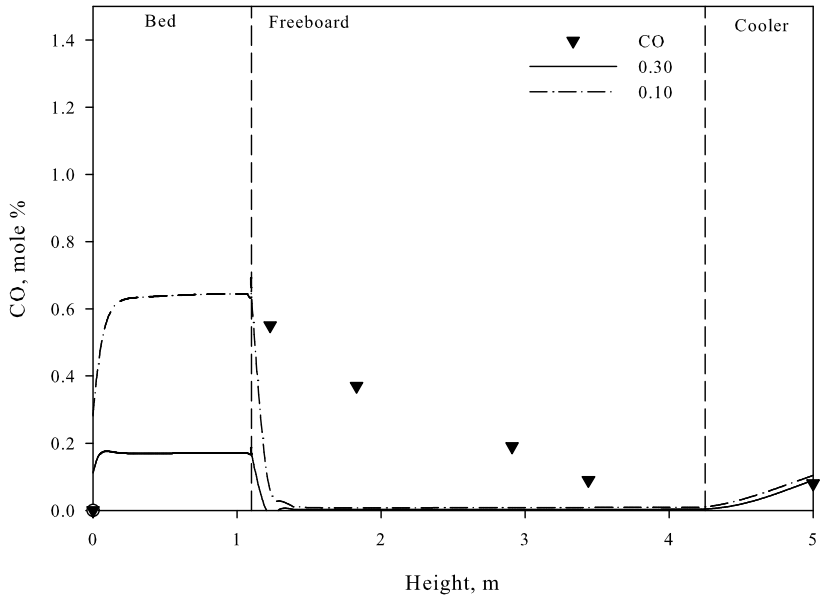

Figure C.3: Effect of scaling the pre-exponential factor on *CO* concentration in Run 5.